Hydrology and
Earth System
Sciences

Improving the hydrological consistency of a process-based solute-transport model by simultaneous calibration of streamflow and stream concentrations

Jordy Salmon-Monviola[1], **Ophélie Fovet**[1], and **Markus Hrachowitz**[2]

[1]UMR SAS, INRAE, Institut Agro, Rennes, France
[2]Department of Water Management, Faculty of Civil Engineering and Geosciences,
Delft University of Technology, Stevinweg 1, 2628 CN Delft, the Netherlands

Correspondence: Jordy Salmon-Monviola (jordy.salmon-monviola@inrae.fr)

Abstract. The consistency of hydrological models, i.e. their ability to reproduce observed system dynamics, needs to be improved to increase their predictive power. As using streamflow data alone to calibrate models is not sufficient to constrain them and render them consistent, other strategies must be considered, in particular using additional types of data. The aim of this study was to test whether simultaneous calibration of dissolved organic carbon (DOC) and nitrate (NO_3^-) concentrations along with streamflow improved the hydrological consistency of a parsimonious solute-transport model. A multi-objective approach with four calibration scenarios was used to evaluate the model's predictions for an intensive agricultural headwater catchment. After calibration, the model reasonably simultaneously reproduced the dynamics of discharge and DOC and NO_3^- concentrations in the stream of the headwater catchment from 2008–2016. Evaluation using independent datasets indicated that the model usually reproduced dynamics of groundwater level and soil moisture in upslope and riparian zones correctly for all calibration scenarios. Using daily stream concentrations of DOC and NO_3^- along with streamflow to calibrate the model did not improve its ability to predict streamflow for calibration or evaluation periods. The approach significantly improved the representation of groundwater storage and to a lesser extent soil moisture in the upslope zone but not in the riparian zone. Parameter uncertainty decreased when the model was calibrated using solute concentrations, except for parameters related to fast and slow reservoir flow. This study shows the added value of using multiple types of data along with streamflow, in particular DOC and NO_3^- concentrations,

to constrain hydrological models to improve representation of internal hydrological states and flows. With the increasing availability of solute data from catchment monitoring, this approach provides an objective way to improve the consistency of hydrological models that can be used with confidence to evaluate scenarios.

1 Introduction

Hydrological models are important tools for short-term forecasting of river flows and long-term predictions for strategic water management planning, as well as for improving understanding of hydrological processes and the complex interactions of water storage and release processes at the catchment scale (Bouaziz et al., 2021; Lan et al., 2020; Minville et al., 2014). In the wide spectrum of modelling, which ranges from simple to complex (Adeyeri et al., 2020; Gharari et al., 2014; Hrachowitz and Clark, 2017), conceptual models are widely used to simulate hydrological dynamics of catchments. In these models, only the dominant processes are represented, and/or several processes may be lumped into a single expression (Pettersson et al., 2001). Conceptualizing the system as a set of storage components connected by flows representing the perceived dominant processes of a catchment provides a certain degree of flexibility. The ability to customize these models to the environmental conditions in a given catchment can ensure an appropriate level of complexity to reproduce response patterns of hydrology and water

quality (Hrachowitz et al., 2016). Major advantages of conceptual models include their relatively low data and computational requirements, which makes them suitable for studies at different scales or for catchments about which little information is available (Gharari et al., 2014; Huang and Bardossy, 2020). However, ad hoc implementation of conceptual models frequently lacks a plausible theoretical basis and thus a meaningful connection of model structure and parameters to observable quantities when representing integrated system processes (Clark et al., 2016). As such, the ability of models, including conceptual ones, to reproduce a system's dynamics is also undermined, not only by random uncertainties in the data but also by epistemic or ontological uncertainties and thus by limited knowledge of the physical processes that underlie the system's response (Beven, 2013; Beven and Westerberg, 2011; Gupta et al., 2012). These uncertainties and the few observations in a continuous spatial domain make such models ill-posed inverse problems (Beven, 2006; Hrachowitz et al., 2014; Pettersson et al., 2001). In hydrology, these insufficient model constraints can result in many equally good alternative model solutions, frequently referred to as equifinality (Beven, 2006). Hydrological models with many parameters thus tend to adapt to errors and to compensate for inadequate representation of processes through the model parameters (Wang et al., 2012). For example, well-predicted river discharge is often associated with poorly predicted evaporation flows because evaporation compensates for errors and closes the hydrological balance (Minville et al., 2014). Thus, deceptively high calibration accuracy may reflect mathematical fitting of an often overparameterized model, which may generate undesirable internal dynamics that decrease accuracy in independent evaluation periods (Fovet et al., 2015a; Hrachowitz et al., 2014). Robust model calibration and evaluation procedures are thus needed to address issues of parameter identifiability (Beven, 2006; Guillaume et al., 2019) and transferability (Hartmann and Bárdossy, 2005; Kreye et al., 2019; Minville et al., 2014) and to avoid models that act as "mathematical marionettes" dancing to match the calibration data (Kirchner, 2006) but often fail to reproduce internal system dynamics.

Recently, a trend toward more comprehensive assessment of the structural adequacy of models has emerged during the calibration process (Rakovec et al., 2016; Yen et al., 2014), with the overall goal of improving the representation of multiple hydrological processes in a model (Clark et al., 2011; Euser et al., 2015; Gupta et al., 2012). The rationale behind this goal is the need to obtain the "right answers for the right reasons" (Blöschl, 2001; Kirchner, 2006), which goes beyond simply comparing model predictions to observed streamflow or associated signature measurements (Euser et al., 2013; Fovet et al., 2015a; Rakovec et al., 2016). Indeed, reflecting the results of many studies, Rakovec et al. (2016) showed that streamflow data are necessary but not sufficient to warrant constraining model components by dividing incoming precipitation among storage, evaporation,

and drainage (Bouaziz et al., 2021). Thus, multiple strategies have been developed to improve the physical realism of conceptual models (i.e. model *consistency*) (Efstratiadis and Koutsoyiannis, 2010), including using additional data that represent internal hydrological states and flows other than streamflow when estimating parameters. Treating the system more holistically (i.e. forcing models to simulate multiple response variables adequately) has considerable potential to improve model accuracy (Hrachowitz et al., 2014). The value of such multi-variable and/or multi-objective strategies has been demonstrated using groundwater levels (Fenicia et al., 2008; Freer et al., 2004; Giustolisi and Simeone, 2006; Molenat et al., 2005), near-surface soil moisture (Brocca et al., 2010; Kunnath-Poovakka et al., 2016; López López et al., 2017; Rajib et al., 2016; Sutanudjaja et al., 2014), saturated contributing areas (Blazkova et al., 2002; Franks et al., 1998; Güntner et al., 1999), snow cover (Bennett et al., 2019; Gao et al., 2017; Riboust et al., 2019), evaporation (Bouaziz et al., 2018; Demirel et al., 2018; Hulsman et al., 2020), streamflow at subcatchment outlets (Moussa et al., 2007), satellite-based total water storage anomalies (Werth and Güntner, 2010; Yassin et al., 2017), and tracer data (Birkel et al., 2011, 2015; Capell et al., 2012; Kuppel et al., 2018a; Piovano et al., 2019; Stadnyk and Holmes, 2023). Alternately, one may seek to extract more information from the available data, for example by developing signatures that represent different aspects of the data (Euser et al., 2013; Fenicia et al., 2018; Gharari et al., 2014), and then compare the signatures of the observed and simulated time series. For streamflow, the hydrological signatures can include quantiles of the streamflow distribution (values of the flow duration curve – FDC), the base flow index, the flashiness index, and many others (e.g. Kavetski et al., 2018).

Simultaneously calibrating hydrological models with streamflow and tracer or other solute concentrations in the stream may decrease their uncertainty and increase their physical plausibility because of the need to reproduce both hydrological and biogeochemical dynamics (Birkel et al., 2017; Fovet et al., 2015b; Pesántez et al., 2023; Pettersson et al., 2001; Strohmenger et al., 2021; Woodward et al., 2013). The value of this strategy has been demonstrated, for example using concentrations of chloride (Hrachowitz et al., 2013) or nitrate (NO_3^-) and sulfate (Hartmann et al., 2013; Pettersson et al., 2001). As the movement of water and solutes through the landscape is inherently coupled (Knapp et al., 2020), using time series of multiple elements along with streamflow during calibration may provide additional insights into the flow paths of water through the catchment (Strohmenger et al., 2021). This potential may be particularly high when using solutes that differ in their sources and flow paths across spatial and temporal scales in a catchment. Calibration that includes streamflow along with solutes that have distinct dynamics, as frequently observed with dissolved organic carbon (DOC) and NO_3^- (Inamdar and Mitchell, 2006; Taylor and Townsend, 2010), such as in headwater agricul-

tural catchments (Aubert et al., 2013; Strohmenger et al., 2020; Thomas et al., 2016), thus has high potential to constrain models to adequately reproduce water storage dynamics and flow paths.

The objective of this study was thus to test the hypotheses that, by including daily in-stream DOC and NO_3^- concentrations simultaneously in a parsimonious conceptual model in a multi-objective and multi-variable calibration and evaluation strategy, we could (1) increase the model's ability to predict streamflow for calibration or evaluation periods, (2) increase the model's internal consistency, and (3) reduce the uncertainty in hydrological parameters.

2   Materials and methods

2.1   Study site

The Kervidy–Naizin catchment is located in western France (48°0′ N; 2°5′ W) (Fig. 1) and forms part of the Agro-Hydro Systems (AgrHyS) Critical Zone Observatory (Fovet et al., 2018). It is a 4.82 km² headwater catchment of the 12 km² Naizin catchment (Fig. 1), which is drained by a second-Strahler-order intermittent stream that frequently dries up from July to October. The climate is temperate oceanic, with a mean ± standard deviation of annual temperature of 11 ± 0.6 °C, annual cumulative rainfall of 894 ± 170 mm yr^{-1}, and specific discharge of 350 ± 140 mm yr^{-1} from 2008–2016. The topography is relatively flat, with few slopes reaching a gradient of 5 %, and an elevation range of 98–140 m a.s.l. (above sea level). The soil is a silty loam 0.5–1.5 m deep, with well-drained Cambisols in the upslope zone and poorly drained Epistagnic Haplic Luvisols and Albeluvisols in the downslope riparian zone (FAO classification; WRB, 2006). At the global scale, Kervidy–Naizin is representative of headwater catchments underlain by bedrock in temperate climates. The bedrock consists of impervious, locally fractured Brioverian schists and lies below a fissured and fractured weathered layer of variable thickness 1–30 m deep (Molenat et al., 2005). A shallow, perennial groundwater body develops in the soil and weathered bedrock. In the upland domain, consisting of well-drained soils, the water table remains below the soil surface throughout the year, varying in depth from 1–5 m (Molenat et al., 2005). In the wetland domain, developed near the stream and consisting of hydromorphic soils (hereafter "riparian zone"), the water table is shallower, remaining near the soil surface generally from October to April/May each year. The seasonal fluctuation of the water table in this catchment has been described as a succession of three hydrological periods (Aubert et al., 2013; Lambert et al., 2013): (i) rewetting of riparian wetland soils after the dry summer season, (ii) rise of groundwater in the upland domain that leads to prolonged waterlogging of wetland soils and establishes a marked hydraulic gradient in groundwater between upland and wetland domains,

and (iii) drawdown of groundwater that leads to drying of the stream (Humbert et al., 2015).

The land use of Kervidy–Naizin consists mainly of agriculture with intensive mixed crop–livestock farming, with maize (36 % of the area), cereals (32 %), and grasslands (13 %) and a high density of livestock (i.e. dairy cattle, pigs and poultry) of five livestock units ha^{-1} (Benoit and Veysset, 2021) according to farm surveys performed in 2008 and 2013 and annual land-use surveys (Casal et al., 2018, 2019; Viaud et al., 2018). From 2002–2015, mean N inputs on the catchment equalled 257 kg ha^{-1} yr^{-1}, coming from slurry and manure fertilization (69 %), inorganic fertilization (21 %, mainly ammonium nitrate), cattle excretion in pastures (5 %), and nitrogen (N) fixation (5 %) (Casal et al., 2019). Kervidy–Naizin is representative of intensive agricultural areas that have an excess of reactive N due to the application of livestock waste and inorganic fertilizers in excess of crop requirements.

In this landscape, most DOC and NO_3^- accumulate in riparian-zone soils and groundwater, respectively (Aubert et al., 2013; Strohmenger et al., 2020). Using end-member mixing analysis to identify DOC sources and quantify their contributions to the DOC stream in Kervidy–Naizin, Morel et al. (2009) estimated that 64 %–86 % of the DOC that entered the stream during storms, when much of the DOC export from soils to streams and rivers occurs (Lambert et al., 2014), came from riparian wetland soil. This result confirmed previous studies that found that riparian soils are the main source of DOC in most headwater catchments (Lambert et al., 2013). Morel et al. (2009) also demonstrated that this riparian wetland zone in Kervidy–Naizin behaved as non-limiting storage of DOC during flushing. Hillslope soils in this catchment also contribute to stream DOC export, but dissolved organic matter (DOM) in upland soils is supply-limited and seasonally depleted after groundwater rises. Upland DOC contribution decreases from ca. 30 % of the stream DOC flow at the beginning of the high-flow period to < 10 % later in this period (Lambert et al., 2013, 2014). In addition, in a high-frequency, multi-solute 10-year monitoring (2000–2010) study of Kervidy–Naizin, Aubert et al. (2013) identified that NO_3^- accumulated in groundwater at a concentration of ca. 20.7 mg N–NO$_3$ L^{-1} compared to 1.6 mg N–NO$_3$ L^{-1} in riparian wetland.

Long-term analysis of the dynamics of nutrient concentrations and hydroclimatic variables at multiple timescales in Kervidy–Naizin highlighted contrasting dynamics of DOC and NO_3^- concentrations due to opposition in their spatial sources. DOC concentrations peaked under wet or storm flow conditions, when NO_3^- concentrations were lowest. In contrast, NO_3^- concentrations peaked under high-water-table and drier conditions, when DOC concentrations were lowest. This opposition between maxima and minima of daily DOC and NO_3^- concentrations can be interpreted as the result of relative mixing contributions of soil-surface riparian flows (i.e. DOC-rich and NO$_3$-poor) and upslope groundwa-
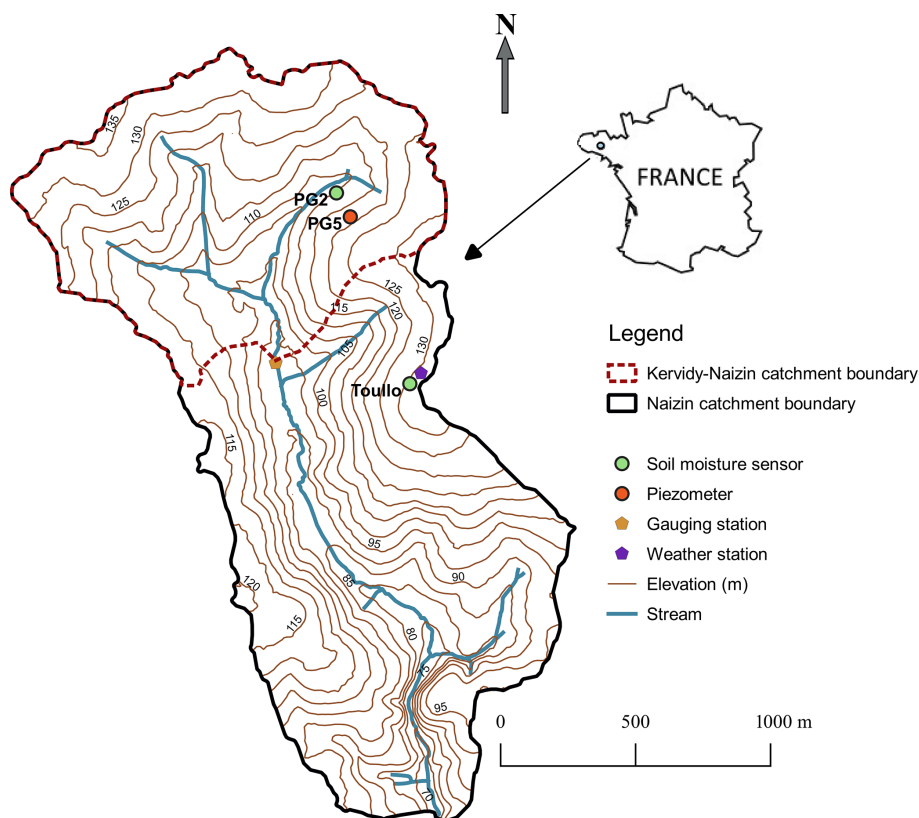
Figure 1. Map of the nested Kervidy–Naizin and Naizin catchments (4.82 and 12.00 km², respectively), in western France. Data from the weather station and Toullo station, which lie outside Kervidy–Naizin but inside Naizin, were used in this study.

ter flows (i.e. NO_3-rich and DOC-poor) (Strohmenger et al., 2020).

2.2   Data monitoring

We used daily aggregated meteorological and streamflow measurements collected from 2002–2017. The weather station in Kervidy–Naizin (Cimel Enerco 516i), located ca. 1 km from the outlet of the catchment (Fig. 1), records hourly rainfall, air and soil temperatures, air humidity, global radiation, wind direction, and wind speed, which allowed for calculation of potential evapotranspiration using the Penman equation (Penman, 1956). Stream level was recorded every minute at the outlet using a float-operated shaft-encoder level sensor and a data logger (Thalimedes OTT) and then converted to streamflow using a rating curve (Carluer, 1998).

Stream water was manually sampled daily at ca. 17:00 LT at the outlet station. These instantaneous grab samples were immediately filtered (pore size: 0.22 μm) on site and stored in the dark at 4 °C in propylene bottles. Analyses were performed within a maximum of 2 weeks. NO_3^- concentrations were measured by ionic chromatography (DIONEX DX 100; ISO 10304, 2007, precision: ±2.5 %). DOC was estimated as total dissolved carbon (C) minus dissolved inorganic C, both

measured using a C analyser (Shimadzu TOC 5050A, precision: ±5 %).

Shallow-groundwater data were collected by a piezometer at mid-slope point (PG5, Fig. 1). The groundwater level at PG5, which has been measured every 15 min (Orpheus OTT) since 2000 using pressure probes, was used because its variations are representative of mean variations in the shallow groundwater in Kervidy–Naizin. The volumetric soil water content was measured in upland and riparian zones of the catchment using time domain reflectometry (TDR) probes. In the upland zone (Toullo station, Fig. 1), it was measured at three depths (i.e. 5, 20, and 50 cm), with three replicates per depth, at 30 min intervals from 1 January 2016 to 1 January 2019; these data were first averaged by depth and then aggregated into daily values. Although the Toullo station lies outside Kervidy–Naizin, we assumed that it could represent Kervidy–Naizin's soil moisture conditions in the upland zone. This assumption is supported by the fact that Kervidy–Naizin and Naizin are nested and have similar characteristics, such as soil types, slopes, and elevation (Matos-Moreira et al., 2017; Sorel et al., 2010). In the riparian zone (point PG2, Fig. 1), the volumetric soil water content was measured at a depth of 5 cm, with three replicates, at 30 min intervals from

3 December 2013 to 1 January 2017; these data were also averaged and then aggregated into daily values.

2.3 Rationale for the solute-transport model

We used a parsimonious semi-distributed solute-transport model, implemented in Python, that was iteratively customized and tested within the DYNAMITE modular modelling framework (Fovet et al., 2015a; Hrachowitz et al., 2014, 2021). The processes are represented by linear or nonlinear equations that connect the flows to model reservoirs (Beven, 2012). This representation of storage–discharge relationships directly connects water flows to biogeochemical processes, which facilitates simultaneous simulation of both water and solute flows (Birkel et al., 2017).

2.3.1 Hydrology

The model spatially distinguishes two functionally distinct response units: hillslope and riparian zones. It represents them as two parallel suites of reservoirs connected by a common groundwater reservoir (Fig. 2). The hillslopes are represented as two reservoirs: the rooting-zone reservoir (S_U) [L] and a fast-responding reservoir (S_F) [L] (e.g. preferential flow structures). As riparian zones often have a distinct hydrological function (Molenat et al., 2005; Seibert et al., 2003, 2009), the model also represents them as two reservoirs: an unsaturated-zone reservoir (S_{UR}) [L] and a fast-responding reservoir (S_R) [L]. The two parallel suites are connected by a slow groundwater reservoir (S_S) [L], characterized by a threshold from which the groundwater feeds the S_{UR} reservoir that represents a groundwater mixing volume (S_{S_mix}) [L]. See Table 1 for the relevant model equations. More detailed model description and justifications for the processes modelled can be found in previous studies (Hrachowitz et al., 2013, 2014, 2015).

The rainfall-runoff model uses daily rainfall (P) [L T^{-1}] and potential evapotranspiration (E_P) [L T^{-1}] to simulate daily specific discharge at the outlet (Q_T) [L T^{-1}]. Upon reaching the soil, P is divided into water that infiltrates into S_U (R_U, Table 1) and excess water by a hillslope runoff-generation coefficient ($C_{H,R}$) routed to S_F (R_F) and S_S (R_P). $C_{H,R}$ is estimated by a logistic function representing the catchment-wide soil-water-holding capacity in the rooting zone (S_{U_max}), which roughly reflects soil water content at field capacity, and a shape factor (β_H). Percolation of water from S_U to S_S (R_{SS}) is estimated by a linear function of the water storage in S_U and a maximum percolation capacity (P_{max}). Evapotranspiration from S_U (E_U) is estimated by a linear function of the relative soil moisture and a transpiration threshold (L_P), which is the fraction of S_{U_max} below which potential evapotranspiration (E_P) is constrained by the water available in S_U.

Fast reservoir S_F receives water (R_F) from S_U (Table 1, Eq. 8) and drains into reservoir S_{UR} according to a linear storage–discharge relationship that is controlled by parameter k_F. Slow reservoir S_S is recharged by R_{SS} and R_P from S_U and slowly drains according to a linear storage–discharge relationship that is controlled by parameter k_S. The water drained from S_S is redistributed between S_{UR} and the stream according to parameter f_{SUR}. Deep-infiltration losses from S_S, represented by calibration parameter Q_L, are used to explicitly represent inter-catchment groundwater flows (i.e. groundwater flows that cross topographic divides), implying that precipitation that falls in one catchment influences the streamflow in another catchment (Bouaziz et al., 2018). Analysis of the long-term water balance of a headwater catchment with similar physiography in Brittany revealed a large deficit (Hrachowitz et al., 2014). There is evidence that many catchments have such deficits, which are caused, at least in part, by large inter-catchment groundwater flow (Hrachowitz et al., 2014; Le Moine et al., 2007), although this cannot be verified completely, as highlighted by Beven (2001). In addition, data from 58 catchments in the Meuse basin indicated that large net inter-catchment groundwater flows likely existed, mainly in small headwater catchments underlain by fractured aquifers (Bouaziz et al., 2018), such as Kervidy–Naizin. The parameter for deep-infiltration losses is also used to reproduce the zero flow at the outlet and groundwater dynamics with a long recession observed during the summer, regardless of the piezometer (Humbert et al., 2015). Consequently, we explicitly modelled inter-catchment groundwater flows for Kervidy–Naizin. Common conceptual models rarely include deep-infiltration losses, which may not prevent them from simulating streamflow accurately but may cause them to misrepresent the natural system, particularly by overestimating actual evaporation rates in compensation (Bouaziz et al., 2018). In the present study, in the absence of detailed knowledge of the underlying processes, deep-infiltration losses from Kervidy–Naizin were conceptualized as a loss term Q_L from S_S.

Riparian reservoir S_{UR} receives water from S_F, S_S, and rainfall (Table 1, Eq. 13). Excess water, estimated using a runoff-generation coefficient ($C_{R,R}$), is routed to S_R (R_R). The water that remains in S_{UR} is available for transpiration (E_{UR}, Table 1, Eq. 14). S_R drains into the stream according to a linear storage–discharge relationship that is controlled by parameter k_R (Table 1, Eq. 18). The total simulated stream discharge equals the sum of slow and fast contributions from S_S and S_R, respectively (Table 1, Eq. 19).

2.3.2 Nitrate transfer and transformation

N inputs to reservoirs S_U and S_{UR} are the daily N surplus (kg N ha^{-1}), which correspond to soil N balances. N inputs consist of inorganic and organic fertilizers (i.e. slurry and manure), biological N fixation, and atmospheric N deposition. N outputs equal the sum of N exported by each crop type. In this study, the N surplus was considered as a net (N inputs − N outputs) diffuse N source for the catch-

Table 1. State and flow equations of the model. See Table A1 for definitions of the variable abbreviations.

Process	Water balance	Eq.	Flow and state equations and relationships	Eq.
Unsaturated zone	$dS_U/dt = P - E_U - R_F - R_P - R_{SS}$	(1)	$E_U = E_P \cdot \min\left(1, \dfrac{S_U}{S_{U\_max}} \dfrac{1}{L_P}\right)$	(2)
			$R_U = (1 - C_{H,R}) \cdot P$	(3)
			$R_F = C_{H,R} \cdot (1 - C_P) \cdot P$	(4)
			$R_P = C_{H,R} \cdot C_P \cdot P$	(5)
			$R_{SS} = P_{max} \cdot \left(\dfrac{S_U}{S_{U\_max}}\right)$	(6)
			$C_{H,R} = \dfrac{1}{\left(1 + \exp\left(\dfrac{-S_U/S_{U\_max} + 0.5}{\beta_H}\right)\right)}$	(7)
Fast reservoir	$dS_F/dt = R_F - R_{FR}$	(8)	$R_{FR} = S_F \cdot \left(1 - e^{-k_F t}\right) dt^{-1}$	(9)
Slow reservoir	$dS_S/dt = (1-f) \cdot (R_{SS} + R_P) - Q_S - R_{SR} - Q_L$	(10)	$Q_S = \begin{cases} (S_S - S_{S\_mix} - Q_L) \cdot (1 - f_{SUR}) \cdot \left(1 - e^{-k_S t}\right) dt^{-1}, & (S_S - S_{S\_mix} - Q_L) > 0 \\ 0, & (S_S - S_{S\_mix} - Q_L) \leq 0 \end{cases}$	(11)
			$R_{SR} = \begin{cases} (S_S - S_{S\_mix} - Q_L) \cdot f_{SUR} \cdot \left(1 - e^{-k_S t}\right) dt^{-1}, & (S_S - S_{S\_mix} - Q_L) > 0 \\ 0, & (S_S - S_{S\_mix} - Q_L) \leq 0 \end{cases}$	(12)
Riparian unsaturated reservoir	$dS_{UR}/dt = P + \dfrac{R_{FR} \cdot (1-f)}{f} + \dfrac{R_{SR}}{f} - E_{UR} - R_R$	(13)	$E_{UR} = E_P \cdot \min\left(1, \dfrac{S_{UR}}{S_{UR\_max}} \dfrac{1}{L_P}\right)$	(14)
			$R_R = C_{R,R} \cdot P$	(15)
			$C_{R,R} = \min\left(1, \left(\dfrac{S_{UR}}{S_{UR\_max}}\right)^{\beta_R}\right)$	(16)
Riparian reservoir	$dS_R/dt = R_R - Q_R$	(17)	$Q_R = S_R \cdot \left(1 - e^{-k_R t}\right) dt^{-1}$	(18)
Total runoff	$Q_T = Q_S + f \cdot Q_R$	(19)		
Total evaporative flows	$E_A = (1 - f) \cdot E_U + f \cdot E_{UR}$	(20)		

Hydrol. Earth Syst. Sci., 29, 127–158, 2025

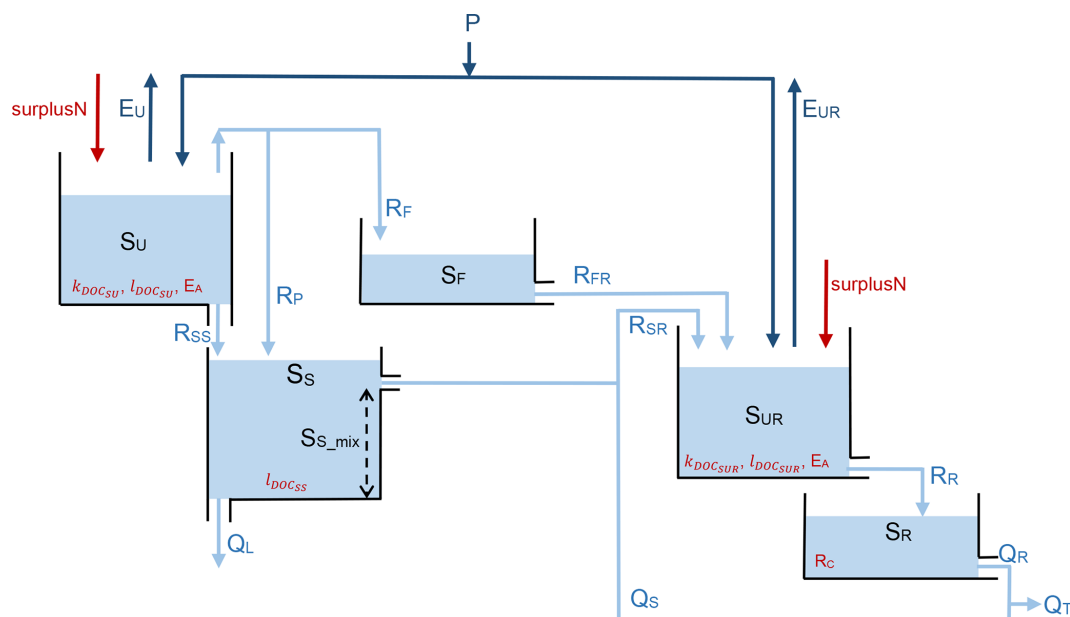https://doi.org/10.5194/hess-29-127-2025

Figure 2. Conceptual model structure used to represent the Kervidy–Naizin catchment. S is storage components, R is recharge flows between reservoirs, Q is liquid flows that leave the system, and E is evaporative flows that leave the system. Dark-blue and light-blue arrows represent water flows and water with solutes, respectively. Biochemical parameters are shown in red for each reservoir. See Table 2 for definitions of the parameters and Table A1 for definitions of the variable abbreviations.

ment (Dupas et al., 2020). Farm surveys performed in 2008 and 2013 led to estimates of a mean annual surplus over the study period (2002—2017) of ca. $90\,\mathrm{kg\,N\,ha^{-1}\,y^{-1}}$ (Casal, 2018). Given the uncertainty in the estimated N surplus, we considered it as a calibration parameter (surplus N, Table 2).

Due to the lack of relevant studies, the period with the highest heterotrophic denitrification rate is unknown for Kervidy–Naizin. In agricultural headwaters, denitrification rates are usually low at the end of winter, increase in spring, peak in summer, and decrease in autumn before reaching their lowest in the middle of winter (Anderson et al., 2014). In agricultural landscapes where N availability exceeds plant requirements, denitrification is mainly limited by C availability, O_2 concentration, and temperature (Barton et al., 1999). Riparian zones of these landscapes often contain large amounts of C. Thus, denitrification rates are expected to be highest from late spring to early autumn, when temperatures are highest and, as long as soils remain wet, O_2 concentrations are lowest (Anderson et al., 2014). We also had no observations of biological transformation of NO_3^- through consumption by aquatic primary producers, although we assumed that it was highest in spring and summer. Thus, in the absence of detailed knowledge of the temporal pattern of biological NO_3^- removal in Kervidy–Naizin, we represented biological transformation of NO_3^- as a constant annual amount of NO_3^- removal (Rc) ($\mathrm{kg\,N\,ha^{-1}\,yr^{-1}}$) from reservoir S_R (Table 2). We assumed that if this constant overestimated the biological NO_3^- removal usually observed in agricultural landscapes in winter, it would influence NO_3^- concentration

little given the Kervidy–Naizin's high NO_3^- load in winter. Thus, representing biological removal as a constant was assumed to be reasonable in a parsimonious model approach (Fovet et al., 2015b).

Denitrification can be a sink for NO_3^- in streams, particularly small (low-order) ones (Böhlke et al., 2009). However, methods for measuring in-stream denitrification are difficult and have high uncertainty, and the controlling variables are not known well enough to make reliable predictions for targeted management decisions (Böhlke et al., 2009). Given the lack of in-stream denitrification observations and the low potential for in-stream NO_3^- removal (estimated at ca. 4 % per year; Salmon-Monviola et al., 2013) in Kervidy–Naizin, we did not model it and thus assumed zero in-stream denitrification.

2.3.3 Dissolved organic carbon transfer and transformation

The conceptualization of biogeochemical processes used to simulate DOC dynamics, similar to that of Birkel et al. (2014), is based on a simple production-loss mass balance and transport along the main flow pathways to the stream. The DOC mass balance ($\Delta M_{\mathrm{DOC}_i}$ [M]) during time step Δt [T] ($\Delta t = 1\,\mathrm{d}$, in this study) of each reservoir i (i.e. S_U, S_{UR} and S_S) differs from more complex C-process models by being simplified into a grouped representation of DOC production (P_{DOC_i} [M]) (processes that transform C were not distinguished) and loss (L_{DOC_i} [M]) (processes that con-

Table 2. Definitions and uniform prior distributions of the parameters of the solute-transport model.

Module	Parameter	Unit	Initial range	Definition
Rainfall–runoff	$S_{\mathrm{U\_max}}$	[mm]	[50–1000]	Storage capacity of the hillslope unsaturated zone
	C_P	[–]	[0.005–1.0]	Preferential recharge coefficient
	β_H	[–]	[0.01–4]	Hillslope runoff coefficient
	$P_{\max}$	[mm d^{-1}]	[0.1–6]	Percolation capacity
	L_P	[–]	[0.01–0.8]	Transpiration threshold
	k_F	[d^{-1}]	[0.001–1]	Storage coefficient of the fast reservoir
	k_S	[d^{-1}]	[0.02–0.06]	Storage coefficient of the slow reservoir
	$S_{\mathrm{S\_mix}}$	[mm]	[500–9000]	Groundwater mixing volume in the slow reservoir
	f_{SUR}	[–]	[0.00001–0.2]	Proportion of water flow from reservoir S_S that passes through reservoir S_{UR}
	Q_L	[mm d^{-1}]	[0.05–1]	Deep infiltration loss
	f	[–]	[0.15–0.30]	Proportion of the catchment covered by the riparian zone
	$S_{\mathrm{UR\_max}}$	[mm]	[50, 500]	Storage capacity in the riparian unsaturated zone
	β_R	[–]	[1–7]	Riparian runoff coefficient
	k_R	[d^{-1}]	[0.04–2]	Storage coefficient of the riparian reservoir
Nitrate	surplus N	[kg N ha^{-1} yr^{-1}]	[50–95]	Nitrogen surplus
	Rc	[kg N ha^{-1} yr^{-1}]	[25–40]	Amount of nitrate removed
Dissolved organic carbon (DOC)	$k_{\mathrm{DOC_{SU}}}$	mg L^{-1}	[15–35]	DOC concentration at which daily DOC is produced in unsaturated storage
	$k_{\mathrm{DOC_{SUR}}}$	mg L^{-1}	[15–35]	DOC concentration at which daily DOC is produced in riparian storage
	E_A	[–]	[1.0–1.2]	Energy parameter
	$l_{\mathrm{DOC_{SU}}}$	[–]	[0–1]	DOC loss in unsaturated storage
	$l_{\mathrm{DOC_{SS}}}$	[–]	[0–1]	DOC loss in slow storage
	$l_{\mathrm{DOC_{SUR}}}$	[–]	[0–1]	DOC loss in riparian storage

sume, retain, and mineralize DOC were not distinguished) (Di Grazia et al., 2023; Koch et al., 2013):

$$\Delta M_{\mathrm{DOC}_i} = P_{\mathrm{DOC}_i} - L_{\mathrm{DOC}_i}. \tag{1}$$

DOC production (P_{DOC_i} [M]) of reservoir i is calculated by multiplying DOC concentration ([DOC]$_i$ [M L^{-1}]) with the total water stored (S_i [L]) at the beginning of each time step. DOC production was assumed to increase as temperature and soil water content increased (Birkel et al., 2020):

$$[\mathrm{DOC}]_i = k_{\mathrm{DOC}_i} \cdot \frac{S_i}{S_{i\_\max}} \cdot E_\mathrm{a}^{(T-\overline{T})}, \tag{2}$$

where k_{DOC_i} [M L^{-1}] is the concentration at which DOC is produced daily in a reservoir i; E_A (dimensionless) is a calibrated temperature-dependent activation energy; T [°C] is the observed daily air temperature; $\overline{T}$ [°C] is the mean annual air temperature for the study period; and $S_{i\_\max}$ and S_i are the capacity [L] and total water stored [L], respectively, of reservoir i. DOC was assumed not to be produced in the groundwater reservoir (S_S), as deeper mineral horizons in soil are considered to be DOC sinks instead (Kalbitz and Kaiser, 2008), and low DOC concentrations have been observed in Kervidy–Naizin's groundwater (mean of ca. 1 mg L^{-1}; Aubert et al., 2013). However, DOC can accumulate in S_S due to recharge from the hillslope reservoir (S_U).

Potential DOC losses (L_{DOC_i} [M]) in the form of mineralization (Köhler et al., 2002), absorption, or consumption in reservoirs S_U, S_{UR}, and S_S are calculated using a loss coefficient (l_{DOC_i}) (dimensionless) (Table 2) applied to the DOC mass of reservoirs at the beginning of each time step.

We assumed that in-stream processes have negligible influence on DOC concentrations. Some studies found that agricultural land use can increase the production of autochthonous DOM in streams (Shang et al., 2018). For example, in an agricultural catchment (Lower Austria, 66 ha), one large DOC source was the stream itself, as in-stream processes caused 37 % of the total DOC load measured at the catchment outlet during base flow conditions from November to May (Eder et al., 2022). Nevertheless, end-member mixing analysis of DOC in Kervidy–Naizin found that stream DOC dynamics during winter storm events could be explained by catchment processes, with little contribution from in-stream sources (Morel et al., 2009). These results confirmed that most of the DOC in streams that drain headwater catchments is likely to be of external origin (i.e. allochthonous), resulting from interactions between biogeochemical and hydrological processes in soils, at least during the wet season (Dalzell et al., 2007; Fovet et al., 2020; Lambert et al., 2013, 2014; Raymond and Saiers, 2010). This is also consistent with the theory of DOM transformation along a fluvial continuum (Creed et al., 2015) and the dynamics of DOM fluorescence observed, for example, by Shang et al. (2018), who found an

increasing contribution of protein-like autochthonous DOM, accompanied by a decreasing contribution of allochthonous DOM, from low-order to high-order systems. For Kervidy–Naizin, these results are supported by two arguments. First, some processes associated with DOC production in summer are unlikely to occur in Kervidy–Naizin's stream, which frequently dries up from July to October. Second, riparian vegetation is dense and covers the entire length of Kervidy–Naizin's network, which decreases primary production of DOC. Thus, we considered the assumption regarding the negligible influence of in-stream processes on DOC concentrations to be valid for Kervidy–Naizin.

The daily solute (NO_3^- or DOC) concentration at the outlet ($C_{out_{solute}}$ [$M L^{-1}$]) is then calculated according to the relative contribution of reservoirs S_S and S_R:

$$C_{out_{solute}} = \frac{C_{solute_{S_S}} \cdot Q_S + C_{solute_{S_R}} \cdot Q_R}{Q_T}.$$ (3)

2.3.4 Mixing assumption

Each reservoir in the model is assumed to be completely mixed to simulate solute dynamics. This approach, used in most studies based on conceptual models (Birkel et al., 2020; McMillan et al., 2012; Pesántez et al., 2023), assumes instantaneous and complete mixing of the incoming water and solute masses in each reservoir, according to a solute-balance equation:

$$\frac{d(c_i \cdot S_i)}{dt} = \sum_j c_{I,j} \cdot I_j - \sum_k c_{O,k} \cdot O_k,$$ (4)

where S_i is the amount of water stored in reservoir i [L], c_i is the associated solute concentration [$M L^{-1}$], I is the j water-inflow [$L T^{-1}$] to a given reservoir (e.g. R_{SS} and R_P from S_U to S_S) (Fig. 2) with the corresponding solute-inflow concentrations $c_{I,j}$ [$M L^{-1}$], and O is the k water-outflow [$L T^{-1}$] from a given reservoir with the corresponding solute-outflow concentrations $c_{O,k}$ [$M L^{-1}$] (e.g. R_{SR} and Q_S from S_S) (Fig. 2).

The model tracks the distribution of ages of the water outflow ($p_{Outflow}(T, t)$, where T is the transit time at time t) (Benettin et al., 2022) using a time stamp for each daily incoming and outflowing water flow in reservoirs, similar to the approach of Birkel and Soulsby (2016). The distribution of ages of water in a reservoir ($p_S(T, t)$) can be derived in a similar way to tracking the ages of water in outflow ($p_{Outflow}(T, t)$), as they are related by a StorAge-Selection (SAS) function developed by Botter et al. (2011):

$$\omega_{Outflow}(T, t) = \frac{p_{Outflow}(T, t)}{p_S(T, t)}.$$ (5)

The SAS function can be considered a statistical summary of the transport behaviour of a hydrological system that quantifies the release of water of different ages from a reservoir to an outflow (Rinaldo et al., 2015). According to the complete mixing assumption of the model, the age distributions of storage and flow are identical to each other (i.e. the outflow composition perfectly represents the storage composition) (Benettin et al., 2022). Thus, the solute concentration of outflow equals the solute concentration of the reservoir. This "well-mixed" situation corresponds to uniform sampling in which $\omega_{Outflow}(T, t) = 1$ and implies that water storage is uniformly sampled by an outflow (Benettin et al., 2013).

2.4 Sensitivity analysis of the solute-transport model

Global sensitivity analysis (GSA) was carried out to determine the effect of the model calibration scenarios on the most sensitive hydrological parameters. GSA allows us to identify the extent to which changes in different parameters influence changes in the hydrological model output and to determine the most important parameters (i.e. that need to be calibrated) and the least important parameters (i.e. that can be fixed as constants) (Reusser et al., 2011; Wang and Solomatine, 2019). GSA, which ranks the relative influence of model parameters on model output (Sun et al., 2022), is generally recommended for hydrological models due to its advantages over local sensitivity analysis methods. Indeed, GSA can consider the influence of input parameters over their entire range of variation and is suitable for non-linear and non-monotonic models, providing results that are independent of modeller bias and a particular site (Song et al., 2015). Among the GSA methods widely applied to hydrological models, we chose a variance-based method as it can provide the most accurate and robust sensitivity indices for complex non-linear models (Reusser et al., 2011; Song et al., 2015; Wang and Solomatine, 2019). Variance-based methods assume that a parameter's influence can be measured by the contribution of the parameter itself or its interactions with two or more other parameters to the variance of the output. The main advantage of variance-based methods is that they can calculate the main and higher-order effects of parameters, which identifies which ones strongly influence the output on their own and which ones strongly influence the output due to their interactions with other parameters (Wang and Solomatine, 2019). We used the Fourier amplitude sensitivity test (FAST) (Saltelli et al., 1999) from the SPOTPY Python framework (Houska et al., 2015) to calculate variance-based sensitivity indices that ranged from 0–1. FAST calculates a first-order sensitivity index (S_i), which measures the effect of each parameter on the output, and a total sensitivity index (S_{T_i}), which measures the effect of each parameter and its interactions with the other parameters on the output (Shin and Kim, 2017). Because S_{T_i} provides more reliable results than S_i when investigating the overall influence of each parameter on the output (Saltelli et al., 2009), we used it to investigate parameter sensitivity, as defined by Saltelli and Annoni (2010):

$$S_{T_i} = \frac{E_{X_{\sim i}} \cdot \left(V_{X_i} \left(Y | X_{\sim i} \right) \right)}{V(Y)}, \tag{6}$$

where X_i is the ith parameter, and $X_{\sim i}$ is the vector of all parameters except X_i.

The variance between parentheses in the numerator denotes that the variance of Y, the value of the scalar objective function, is considered over all possible values of X_i while keeping $X_{\sim i}$ fixed. The expectation operator outside the parentheses is considered over all possible values of $X_{\sim i}$, while the variance $V(Y)$ in the denominator is the total (unconditioned) variance (Shin and Kim, 2017). The numerator represents the expected variance if all parameters except X_i are fixed (Saltelli and Annoni, 2010).

Calculating S_{T_i} for a single parameter requires $n \times (p + 2)$ model runs, where n is the sample size and p is the number of parameters (Saltelli, 2002). To determine an appropriate sample size for this GSA, we relied on the experiment of Nossent et al. (2011), in which the sensitivity index did not converge until $n = 12\,000$; thus, with 14 hydrological parameters, we performed $192\,000$ model runs. In this GSA, the Nash–Sutcliffe model efficiency coefficient (Nash and Sutcliffe, 1970) was used to assess daily streamflow output, as suggested by Nossent et al. (2011).

2.5 Model calibration and evaluation

To limit adverse effects of equifinality and ensure robust posterior parameter distributions to represent processes meaningfully, extensive multi-objective and multi-variable calibration was performed by calibrating hydrological and biogeochemical model predictions simultaneously. When using multi-objective optimization to calibrate a model, the goal is to find a set of solutions that simultaneously optimize several, potentially conflicting, objective functions that measure individual processes. The interaction of multiple objectives leads to a set of compromised solutions known as Pareto-optimal front (Mostafaie et al., 2018). As none of the solutions can be considered superior when there is more than one objective to optimize, Pareto-optimal solutions (hereafter "Pareto front") are also called non-dominated solutions (Yeste et al., 2023) with equally good parameter sets, which provides an uncertainty boundary of the predictive model. The caRamel algorithm (Monteil et al., 2020) used in this approach combines the multi-objective evolutionary annealing-simplex algorithm (Efstratiadis and Koutsoyiannis, 2008) and the non-dominated sorting genetic algorithm II (Reed and Devireddy, 2004). The caRamel algorithm produces an ensemble of parameter sets (i.e. a "generation") to run the model, downscales the generation to the parameter sets that optimize the objective functions, and generates a new parameter set that produces more accurate results.

The research hypotheses of this study were tested using a stepwise strategy with four model calibration scenarios based on different combinations of model-performance metrics (Table 3):

- scenario 1 (S1) – only data on streamflow used for calibration, with six metrics used to describe the predicted streamflow signatures;

- scenario 2 (S2) – data on streamflow and stream DOC concentration used for calibration, with two metrics including the mean of the metrics in S1 and the Kling–Gupta efficiency (Gupta et al., 2009) used to assess the predicted DOC concentrations;

- scenario 3 (S3) – same as S2 but the solute was NO_3^- instead of DOC;

- scenario 4 (S4) – data on streamflow and stream DOC and NO_3^- concentrations used for calibration, with three metrics including the mean of the metrics in S1 and the Kling–Gupta efficiency used to assess the predicted DOC and NO_3^- concentrations.

The calibration period was set from 1 January 2013 to 1 September 2016, while the evaluation period was set from 1 August 2008 to 31 December 2011, each simulated after 3 years of initialization. These periods, the same as those of Strohmenger et al. (2021), were chosen to be able to compare model performance to two approaches to solute modelling. The hydrological year 2012 was excluded from these periods due to a problem with laboratory analysis of NO_3^- concentrations that year. The uniform prior parameter distributions were based on previous studies of headwater catchments in similar physiographic contexts (Fovet et al., 2015a; Hrachowitz et al., 2015) (Table 2). The prior distribution of storage coefficient k_S had been narrowly constrained based on previous baseflow-recession analysis using a correlation method (Yang et al., 2018). Three prior parameter constraints (Gharari et al., 2014; Hrachowitz et al., 2014) were added to the calibration algorithm to reduce parameter uncertainties: $k_S < k_F$, $k_F < k_R$, and $S_{UR\_max} < S_{U\_max}$.

Up to $70\,000$ model runs were used for each calibration scenario, with several successive optimizations to confirm reproducibility of the results, as recommended by Monteil et al. (2020). All parameter sets that belonged to the final Pareto fronts (hereafter, "envelope") were retained as feasible solutions for each calibration scenario (Table 3). To illustrate the results for the predicted discharges and solute concentrations, a "best-compromise" set was selected from the Pareto front that minimized the Euclidean distance to the optimal point in the multi-objective space of each calibration scenario. All simulated discharges and concentrations using all parameter sets of the Pareto front provided information about the uncertainty in the model's output.

In the later evaluation step, observed soil water content and groundwater level measurements were used as independent data to assess the consistency of internal processes of the best-compromise model for each scenario.

Table 3. Signatures for streamflow, dissolved organic carbon (DOC), and nitrate (NO_3^-) and the associated performance metrics used for model calibration scenarios and evaluation. The size of the Pareto front was the number of solutions. NSE – Nash–Sutcliffe model efficiency coefficient, KGE – Kling–Gupta efficiency.

Calibration scenario	Variables/signatures	Abbreviation	Performance metrics	Size of the Pareto front	References
S1: streamflow only	Time series of streamflow	Q $\log(Q)$	NSE_Q, KGE_Q $NSE_{\log Q}$		Gupta et al. (2009), Nash and Sutcliffe (1970)
	Flow duration curve	FDC	NSE_{FDC}	280	Jothityangkoon et al. (2001), Sawicz et al. (2011)
	Runoff ratio	RUNOFF	NSE_{RUNOFF}		Sawicz et al. (2011), Yadav et al. (2007)
	Volumetric efficiency	VE	VE_Q		Criss and Winston (2008)
S2: streamflow and DOC	Streamflow DOC	Q DOC	Mean of metrics of S1 KGE_{DOC}	180	Gupta et al. (2009)
S3: streamflow and NO_3^-	Streamflow NO_3^-	Q NO_3^-	Mean of metrics of S1 KGE_{NO_3}	110	Gupta et al. (2009)
S4: streamflow, DOC and NO_3^-	Streamflow DOC NO_3^-	Q DOC NO_3^-	Mean of metrics of S1 KGE_{DOC} KGE_{NO_3}	270	Gupta et al. (2009) Gupta et al. (2009)

Soil moisture is a key variable for the energy and water balance at the land surface. It affects the partitioning of solar radiation into latent and sensible heat as well as the partitioning of precipitation into direct runoff and catchment storage (Duethmann et al., 2022). Accurate prediction of soil moisture is thus essential for simulating streamflow, evapotranspiration, and percolation (Rajat and Athira, 2021; Rajib et al., 2016) and for constraining the parameters of hydrological models. The role of groundwater in the seasonal and multi-year dynamics of streamflow is also essential: in many temperate catchments, groundwater stores water during wet periods and releases it throughout the year, thus contributing greatly to low flows (Pelletier and Andréassian, 2022). These variables are important for characterizing the internal hydrological dynamics of a catchment and are therefore relevant for assessing the internal consistency of the model.

The data observed for soil water content at Toullo and PG2 were normalized (from 0–1) as a function of their minimum and maximum values over all of the periods studied. All normalized data observed at Toullo station and point PG2 were compared to the normalized simulated water content in the hillslope reservoir (S_U) and riparian reservoir (S_{UR}), respectively. To compare to the observed groundwater level, the simulated groundwater level was estimated from simulated water storage in the groundwater reservoir (S_S) (Seibert, 2000) using the exponential function $z = -e^{A \cdot S_S + B}$, where S_S is water storage in the slow reservoir, and z is the groundwater level. Coefficients A and B were determined by linear regression between the simulated water storage and the observed groundwater level. The non-parametric Mann–Whitney U test was used to test whether model predictions of calibration scenarios S2, S3, and S4 differed significantly ($p < 0.05$) from those of the baseline scenario S1.

3 Results

3.1 Global sensitivity analysis of parameter influence on streamflow

The hydrological parameters that influenced predicted streamflow the most were related to recharge (C_P; $S_T = 0.59$), deep-infiltration losses (Q_L; $S_T = 0.25$), percolation capacity (P_{max}; $S_T = 0.18$), storage capacity of the hillslope unsaturated zone (S_{U_max}; $S_T = 0.15$), and storage coefficient of the fast-responding reservoir in the riparian-zone reservoir (k_R; $S_T = 0.14$) (Fig. 3). The strong influence of C_P was logical, as it determines the recharge from S_U to S_S and S_{UR} to S_R (i.e. how water from runoff is redistributed between the riparian zone and groundwater). Parameters related to the area of the riparian zone (f) and the transpiration threshold (L_P) had less influence.

3.2 Prediction of streamflow and solute concentrations

Overall, the model reproduced the main features of the observed hydrological response (Fig. 4) in both the calibration (NSE_Q, $NSE_{\log Q}$, and $KGE_Q > 0.8$) and evaluation (NSE_Q, $NSE_{\log Q}$, and $KGE_Q > 0.7$) periods for all scenarios. The predicted streamflow reproduced the seasonal dynamics observed during the wetting-up (rising limb of the hydrograph), wet, and recession periods. The high flow variations associated with storm events were usually represented relatively well ($NSE_Q > 0.75$) in calibration and evaluation periods, with good synchronicity, particularly in winter 2010 and 2014. Overall, model performances for the evaluation period were only slightly lower than those for the calibration period for all four scenarios (Figs. 4 and A1). Performance of the best-compromise model was slightly higher
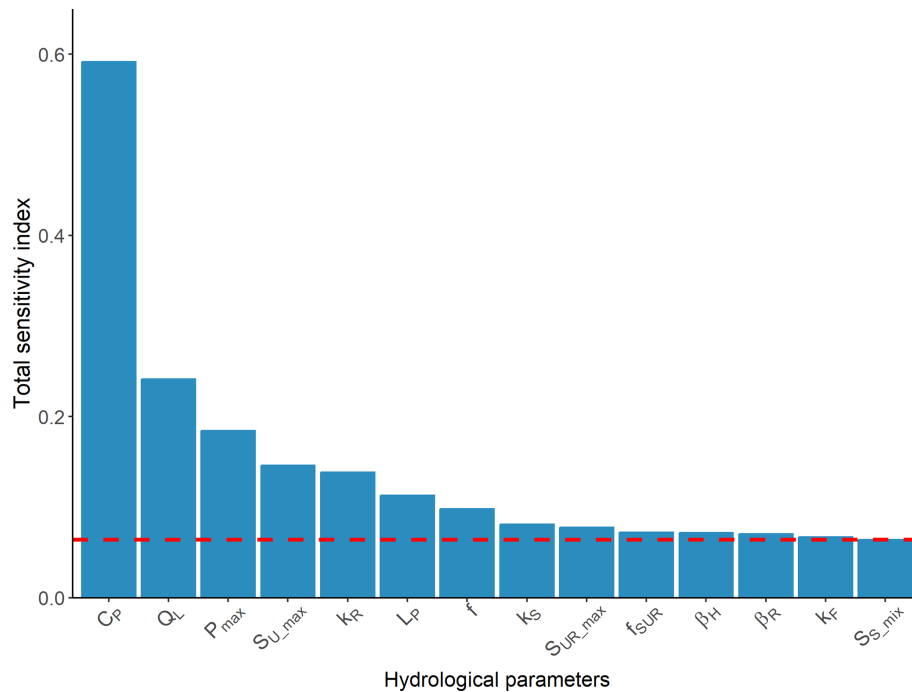
Figure 3. Total sensitivity indices estimated using the Fourier amplitude sensitivity test of the influence of hydrological parameters on predicted streamflow. The dashed red line represents the minimum total sensitivity index.

for S1 than for the other scenarios, for both calibration and evaluation periods (Fig. 4). The difference in performance between S1 and S2 was smaller. The uncertainty in predicted streamflow estimated from the envelope was low for the calibration and evaluation periods but appeared to peak during low flow periods. The calibrated model provided similarly reasonable representations of DOC (Fig. 5) and NO_3^- (Fig. 6) concentrations. Predicted DOC concentrations for the calibration period were slightly more accurate for S2 (Fig. 5a) than for S4 (Fig. 5b). Predicted NO_3^- concentrations for the calibration period were slightly more accurate for S3 (Fig. 6a) than for S4 (Fig. 6b). The model reproduced the contrasting dynamics of stream DOC and NO_3^- (Aubert et al., 2013; Strohmenger et al., 2020), with maximum DOC and minimum NO_3^- concentrations occurring in autumn. During this period, the median simulated DOC concentration was ca. $8.7\,\mathrm{mg\,L^{-1}}$, while that of NO_3^- concentration was ca. $11\,\mathrm{mg\,N{-}NO_3\,L^{-1}}$. During the wetting-up period, DOC concentrations decreased to a median of 2.5–$3.5\,\mathrm{mg\,L^{-1}}$, while NO_3^- concentrations increased to a median of 14–$16\,\mathrm{mg\,N{-}NO_3\,L^{-1}}$. These concentrations remained relatively stable during the wet and recession periods. At the end of the recession period, DOC concentration increased slightly to a median of ca. 5.5–$6\,\mathrm{mg\,L^{-1}}$, while NO_3^- concentration decreased to a median of ca. $12\,\mathrm{mg\,N{-}NO_3\,L^{-1}}$. The model simulated high NO_3^- concentrations in summer, when streamflow and NO_3^- concentrations had not been observed. During summer dry periods, the stream effec-

tively dries up, and no water flows at the outlet, which made it more difficult to calibrate the model to predict their solute concentrations. The model simulated near-zero water flow during dry periods but occasionally simulated flow on certain days when zero flow had been observed, which yielded relatively high simulated NO_3^- concentrations. The lack of observed NO_3^- concentrations during dry periods also provided no constraints that could help the model represent NO_3^- concentrations realistically.

The simulated hydrological signatures for all solutions on the Pareto front provide evidence that including solute data in the calibration improves the ability of the model to reproduce certain streamflow characteristics. While the performance based on median hydrological metrics (NSE_Q, $NSE_{\log Q}$, KGE_Q, VE_Q, NSE_{FDC}) was lower overall for S2 and S4 than for S1 for both calibration and evaluation periods (Fig. 7), the median NSE runoff ratio (NSE_{RUNOFF}) was significantly higher for S4 than for S1 for the evaluation period (Fig. 7b). In contrast, the performance was significantly higher for S3 than for S1 based on median $NSE_{\log Q}$ and VE_Q metrics for the calibration period and on median NSE_Q, $NSE_{\log Q}$, VE_Q, and NSE_{RUNOFF} metrics for the evaluation period. These results suggest that simultaneously evaluating model predictions of streamflow and NO_3^- concentration improves the model's ability to reproduce streamflow, especially low flows, due to the improvement in $NSE_{\log Q}$. Compared to S1, the model's hydrological performance decreased the most for S2 and the least for S3. The hydrological
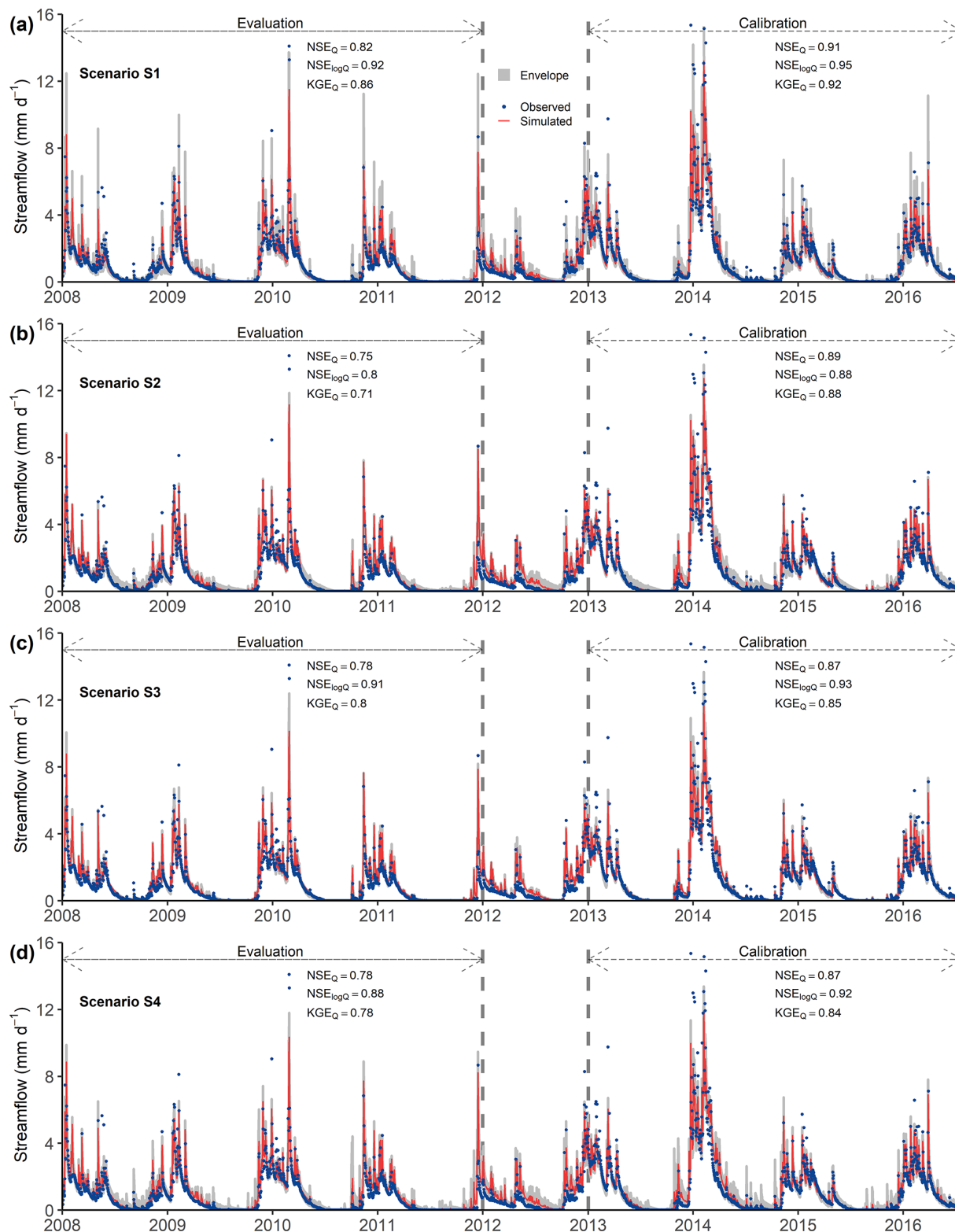
Figure 4. Observed and simulated flows for the calibration and evaluation periods according to the four scenarios: **(a)** S1 (streamflow only), **(b)** S2 (streamflow + dissolved organic carbon (DOC)), **(c)** S3 (streamflow + nitrate (NO_3^-)), and **(d)** S4 (streamflow + DOC + NO_3^-). The simulated data for each scenario correspond to the best-compromise simulated discharge of the set of optimal solutions. "Envelope" refers to the simulated discharge envelope using all parameter sets on the Pareto front. See Table 3 for definitions of model-performance metrics.
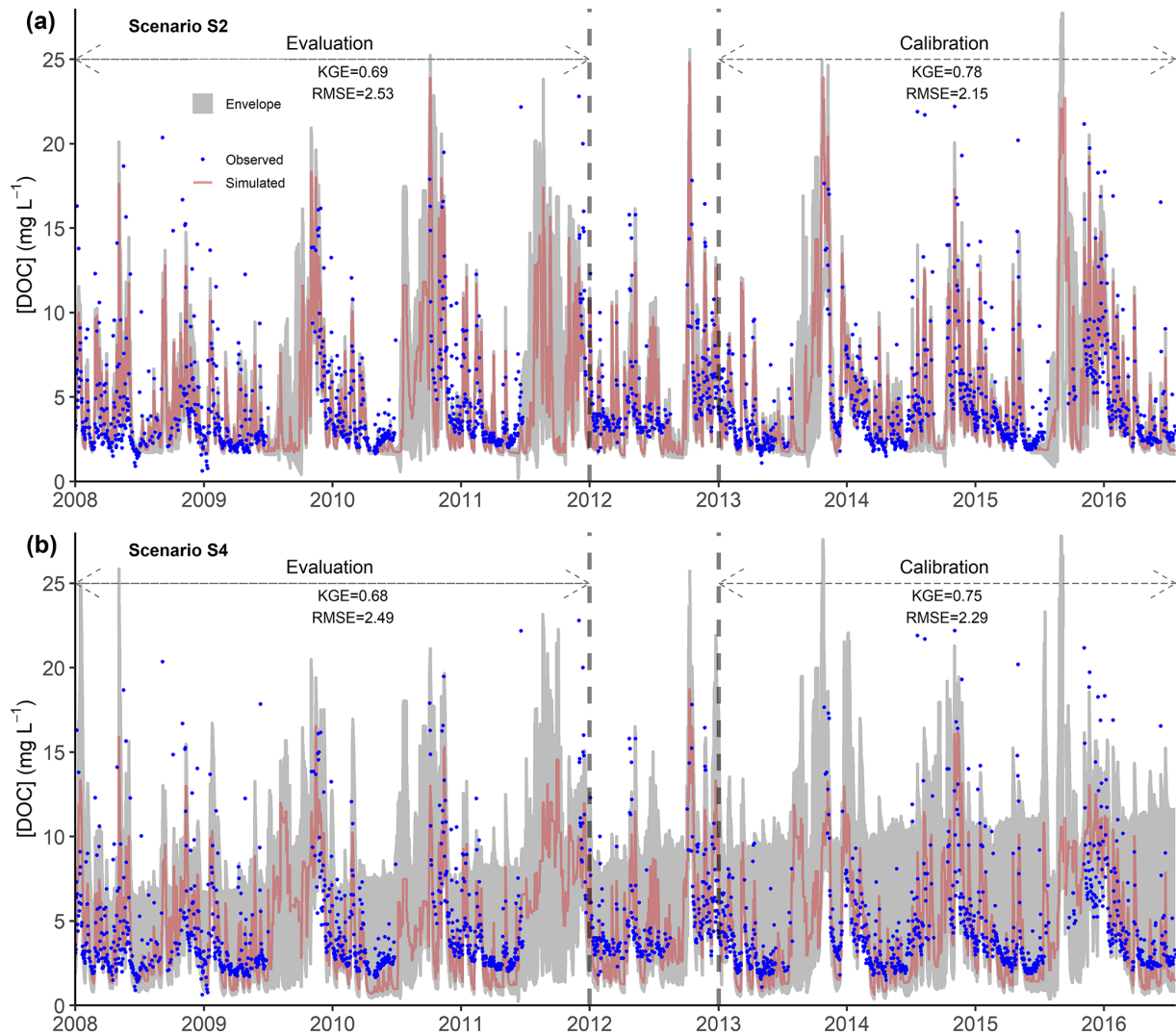
Figure 5. Observed and simulated dissolved organic carbon (DOC) concentrations for the calibration and evaluation periods according to two scenarios: **(a)** S2 (streamflow + DOC) and **(b)** S4 (streamflow + DOC + NO_3^-). The mean ($\pm$ standard deviation) observed DOC concentration was 4.8 ± 3.5 and 4.5 ± 3.1 mg DOC L^{-1} for the calibration and evaluation period, respectively. The simulated data for each scenario correspond to the best-compromise simulated DOC concentration of the set of optimal solutions. "Envelope" refers to the simulated DOC concentration envelope using all parameter sets on the Pareto front. KGE – Kling–Gupta efficiency, RMSE – root-mean-square error. See Table 3 for definitions of model-performance metrics.

metrics for S2 also had wider ranges than those for the other scenarios.

Including DOC concentration with streamflow in the calibration showed lower performance for S4 than for S2, while that using NO_3^- concentration showed lower performance for S4 than for S3 (Fig. 7). These results, consistent for both calibration and evaluation periods, supported the observations (Figs. 5 and 6), which suggests that calibrating the model with each solute individually with streamflow better reproduced solute concentrations than calibrating the model with all solutes and streamflow simultaneously.

3.3   Effects on the distribution of hydrological parameters

Overall, the posterior distribution of hydrological parameters differed among the four calibration scenarios (Fig. 8), except for f_{SUR} and k_R, which were less sensitive to the calibration method (i.e. similar optimal values and distributions), indicating that they had been identified well (Fig. 8i and n). For some parameters, the distributions differed only for one scenario, such as S_{U_max} for S3 (Fig. 8a) and P_{max} for S3 (i.e. smaller values and a narrower range of uncertainties compared to other scenarios, considering both the interquartile range and the total whisker range) (Fig. 8d). The latter
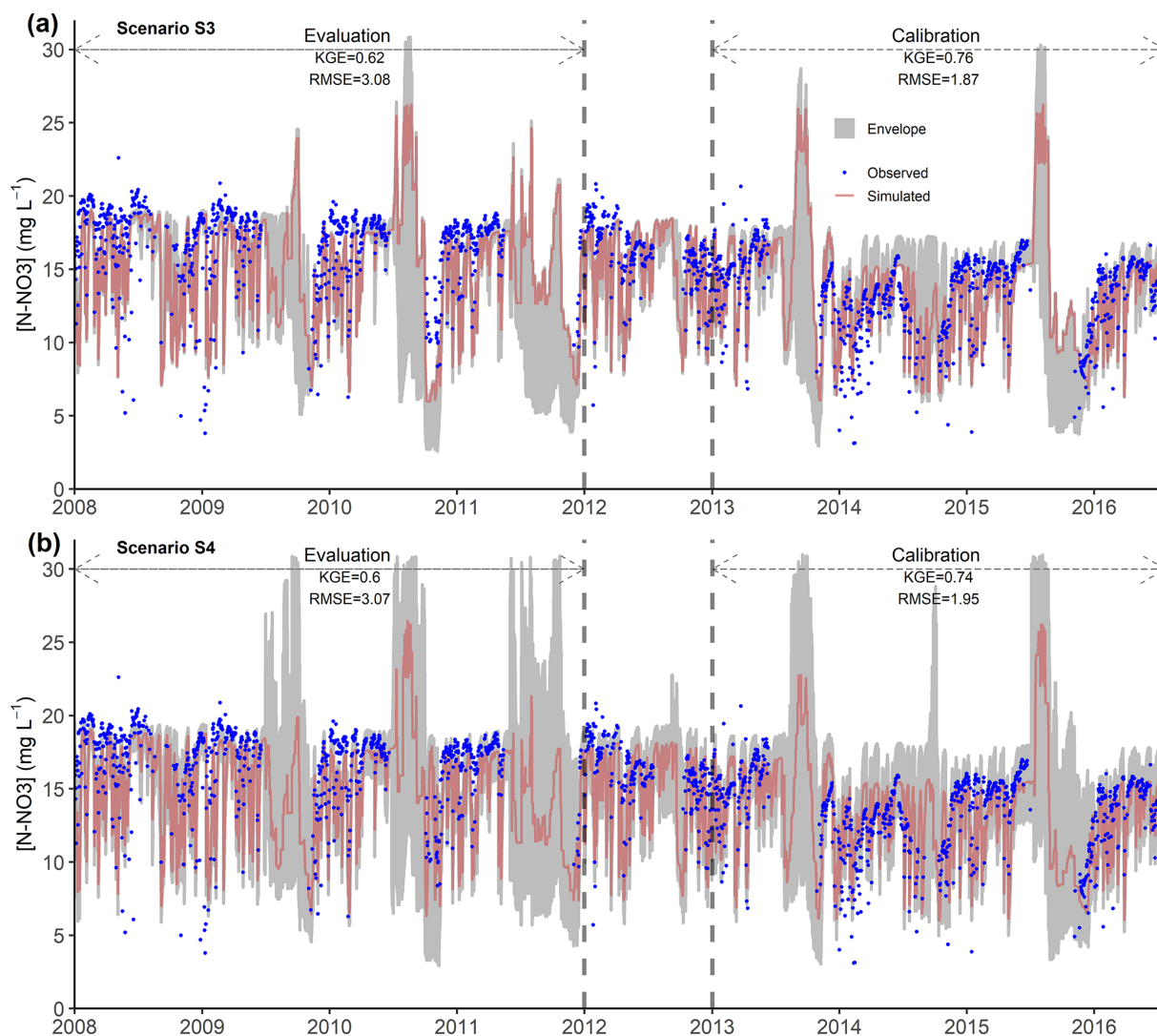
Figure 6. Observed and simulated nitrate (NO_3^-) concentrations for the calibration and evaluation periods according to two scenarios: **(a)** S3 (streamflow $+ NO_3^-$) and **(b)** S4 (streamflow $+$ DOC $+ NO_3^-$). The mean ($\pm$ standard deviation) observed NO_3^- concentration was 13.4 ± 2.7 and 16.6 ± 2.8 mg N–NO$_3$ L^{-1} for the calibration and evaluation period, respectively. The simulated data for each scenario correspond to the best-compromise simulated NO_3^- concentration of the set of optimal solutions. "Envelope" refers to the simulated NO_3^- concentration envelope using all parameter sets on the Pareto front. KGE – Kling–Gupta efficiency, RMSE – root-mean-square error. See Table 3 for definitions of model-performance metrics.

suggests that calibration using NO_3^- concentration strongly influenced soil parameters, decreasing percolation of water from S_U to S_S. Similarly, the distribution of S_{UR_max} for S2 differed from other scenarios and had a narrower range of uncertainties, considering both the interquartile range and the total whisker range. This suggests that calibration using DOC concentration improved identification of S_{UR_max} (Fig. 8l) and that reservoir S_{UR} needs a lower capacity to reproduce both streamflow and DOC concentrations. In addition, for S4, distributions of the most influential hydrological parameters (i.e. C_P and Q_L) (Fig. 8b and j), as well as of groundwater parameters k_S and S_{S_mix}, differed from those of

the other scenarios. Comparing distributions of the groundwater mixing volume in the slow reservoir (S_{S_mix}) for S2 and S3 showed that its size could be decreased by a factor of ca. 3 when calibrating using NO_3^- concentrations instead of DOC concentrations (Fig. 8h).

Overall, all parameters except for k_F and k_S had lower uncertainty when the model was calibrated using solute concentrations, whether simultaneously or separately (Fig. 8). More specifically, the uncertainty in β_H, f_{SUR}, S_{S_mix}, and k_R decreased for S2, S3, and S4. The uncertainty in C_P, β_R, and S_{UR_max} decreased for S2 and S3, while that in P_{max} and L_p decreased for S3 and S4. The uncertainty in S_{U_max} de-
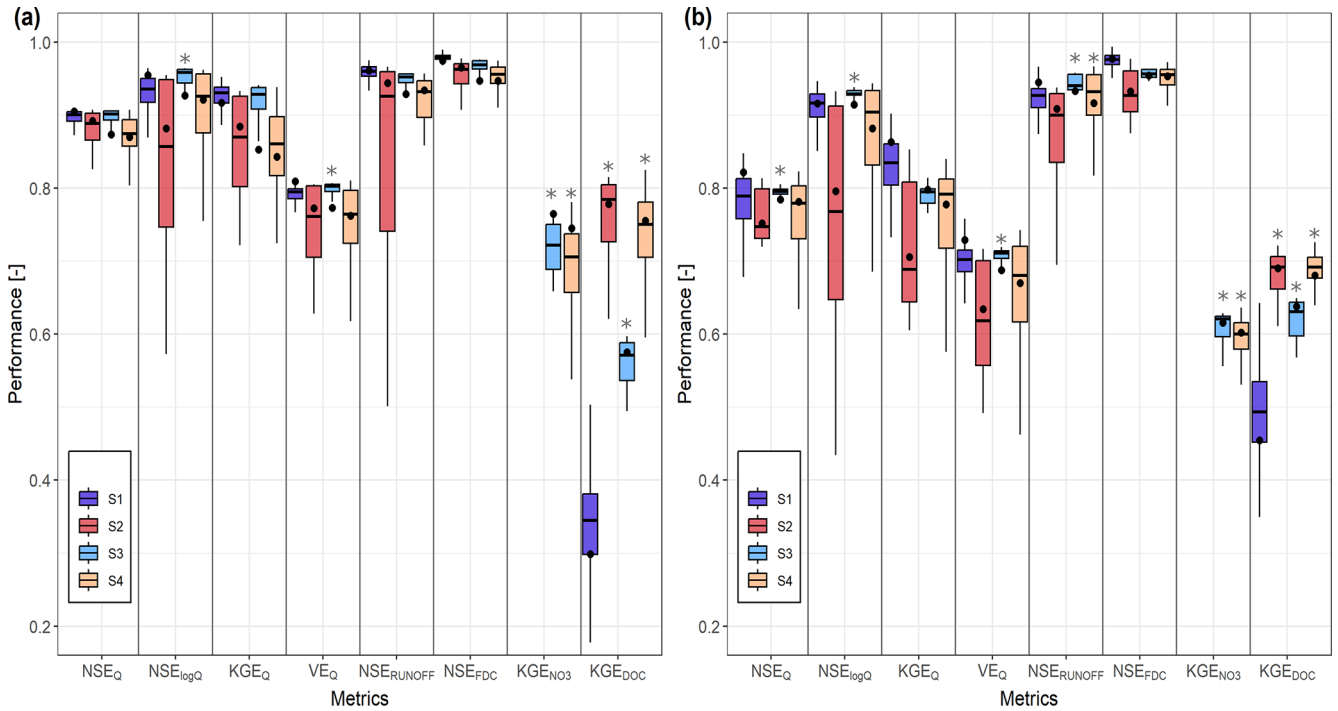
Figure 7. Box plots of performance metrics for predictions of hydrological and solute concentration according to four scenarios: S1 (streamflow only), S2 (streamflow + DOC), S3 (streamflow + NO_3^-) and S4 (streamflow + DOC + NO_3^-) for the **(a)** calibration period and **(b)** evaluation period. Whiskers represent 1.5 times the interquartile range. Black circles indicate the best-compromise solution of the Pareto front. The box plots of KGE_{NO_3} for scenarios S1 and S2 are not shown, as their values were negative (median $= -1$) because the model was not calibrated to represent NO_3^- concentrations in these scenarios. An asterisk above a box plot indicates values significantly ($p < 0.05$) larger than those for scenario S1 (one-sided Mann–Whitney test). See Table 3 for definitions of model-performance metrics.
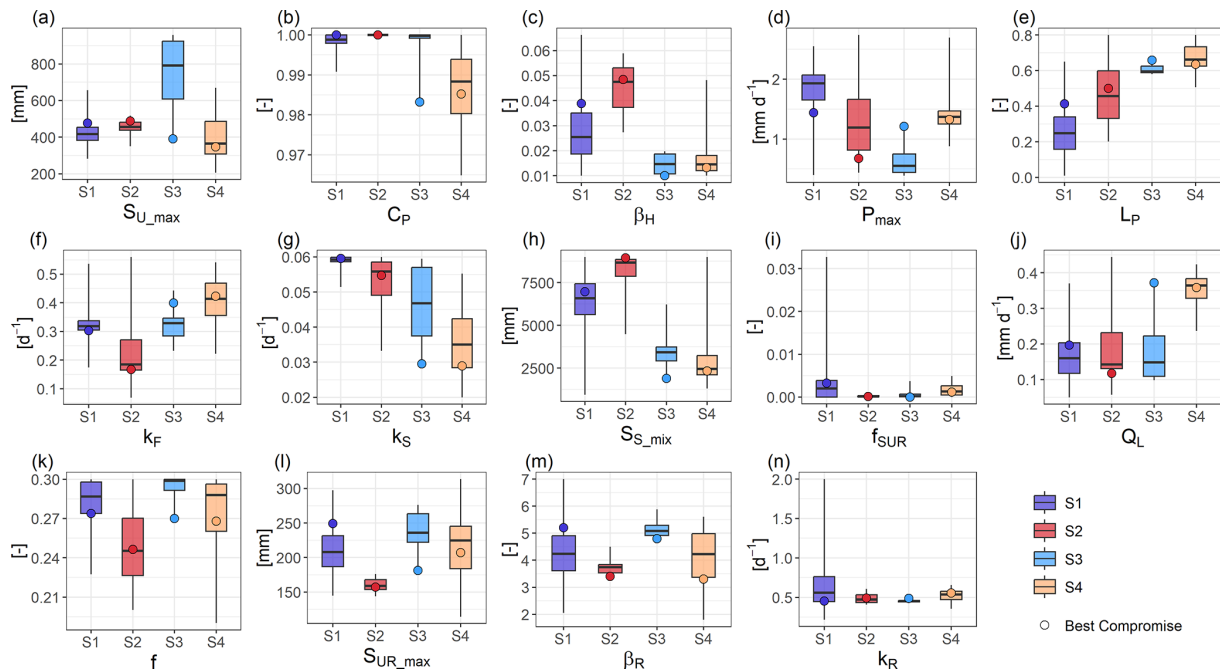
Figure 8. Box plots of hydrological parameters values for the four scenarios: S1 (streamflow only), S2 (streamflow + DOC), S3 (streamflow + NO_3^-), and S4 (streamflow + DOC + NO_3^-). Whiskers represent 1.5 times the interquartile range. The circle on each box plot indicates the parameter's value in the best-compromise set on the Pareto front for each scenario.

creased only for S2, while that in f decreased only for S3. For deep-infiltration losses (Q_L), only calibration using DOC and NO_3^- concentrations simultaneously (S4) decreased its uncertainty compared to those for other scenarios (Fig. 8j).

3.4 Internal model states and consistency

3.4.1 Groundwater level

Overall, the calibration that included solute concentrations with streamflow (S2, S3 and S4) significantly improved simulation of groundwater level compared to S1 (Fig. 9). In S1, performance metrics NSE and KGE were indeed the lowest, and PBIAS (percent bias; Moriasi et al., 2007) and RMSE were the highest. S3 and S4 reproduced groundwater levels (NSE = 0.92 and 0.93, respectively) better than S2, while S3 reproduced best the low groundwater levels in 2009, 2011, and 2013. However, for S3 and S4, the model tended to slightly overestimate the low groundwater levels in 2010 and 2015. Overall, the model reproduced the observed magnitude and seasonality of the groundwater level relatively well (NSE = 0.76–0.93, depending on the scenario). PBIAS values were negative for all scenarios, indicating that the model tended to underestimate groundwater level.

3.4.2 Soil moisture

Overall, calibrating the model with streamflow and solute concentrations simultaneously did not improve simulation of soil moisture dynamics in the riparian zone compared to S1 (Fig. 10a). The calibration that included DOC concentrations with streamflow (S2) had significantly lower performance to reproduce normalized soil moisture at PG2 (NSE = 0.58 and KGE = 0.74) compared to S1. The model reproduced observed soil moisture better when it was calibrated using DOC and NO_3^- simultaneously (S4, with NSE = 0.73 and KGE = 0.78) than when using only one solute (S2 or S3, with NSE = 0.58 and 0.69, respectively, and KGE = 0.74 and 0.75, respectively). The model reproduced major features of the observed dynamics of normalized soil moisture at PG2 (i.e. the riparian zone) (NSE = 0.58–0.79, depending on the scenario). It also reproduced drying rates at the end of the summer and wetting rates well overall. However, the model tended to slightly underestimate soil moisture in summer 2015 and winter 2016. PBIAS values were negative for all scenarios, indicating that the model tended to underestimate normalized soil moisture at PG2.

Only S2 reproduced soil moisture in the upslope zone significantly better than S1 did (NSE = 0.94 and 0.92, respectively) (Fig. 10b). For S3 and S4, the model did not reproduce the wetting rate well at the beginning of 2017, when it overestimated soil moisture. S3 and S4 had significantly lower performance than S1 did. Overall, the model reproduced the observed dynamics of normalized soil moisture at

Toullo (i.e. the upslope zone) (NSE = 0.79–0.94, depending on the scenario).

3.5 Water balances

Calibrating the model with DOC and NO_3^- concentrations along with streamflow data influenced water-balance components and changed the storage in reservoirs S_U, S_S, and S_{UR}. The median simulated total evaporative flow (E_U and E_{UR}) was highest for S1 (470 mm yr^{-1}) and lowest for S4 (372 mm yr^{-1}) (Fig. 11a). Median deep-infiltration losses (Q_L) were highest for S4 (128 mm yr^{-1}) and lowest for S3 (54 mm yr^{-1}). The median contribution of S_R to discharge (Q_R) was slightly but significantly higher for S3 and S4 (108 and 109 mm yr^{-1}, respectively) than for S1 (100 mm yr^{-1}). The median contribution of S_S to discharge (Q_S) was significantly higher for S2 (293 mm yr^{-1}) than for S1 (242 mm yr^{-1}). S_S and S_{UR} stored water during the simulation, while S_U lost water. S_S tended store significantly more water for S4 (2.7 mm yr^{-1}) than it did for S1 (1.2 mm yr^{-1}) (Fig. 11b). S_U lost significantly more water for S3 (−21 mm yr^{-1}) than for S1 (−12 mm yr^{-1}) and lost the least for S4 (−10.6 mm yr^{-1}).

4 Discussion

4.1 Effect on streamflow, groundwater and soil moisture

The parsimonious solute-transport model reasonably reproduced simultaneously the dynamics of discharge, DOC and NO_3^- concentrations in the stream of the Kervidy–Naizin catchment for all scenarios. Model predictions based on independent data indicated that the model generally reproduced the dynamics of groundwater level and soil moisture in upslope and riparian zones for all scenarios. Including solute (DOC and NO_3^-) data along with streamflow data in a multi-objective calibration strategy improved the representation of groundwater storage and soil moisture in the upslope zone (Figs. 9 and 10b). The improvement in the representation of groundwater level was significant and relatively large for scenarios S2, S3, and S4 compared to S1 (Fig. 9). In contrast, the improvement in the representation of soil moisture in the upslope zone was significant but relatively small only for scenario S2 compared to S1 (Fig. 10b). Thus, only scenario S2 improved the representation of both groundwater and soil moisture in the upslope zone.

Studies have shown that using additional information to constrain hydrological models usually improves spatial and/or temporal patterns of internal state variables and flows but does not necessarily improve the accuracy of predicted runoff (López López et al., 2017; Tong et al., 2021). Woodward et al. (2013) developed a catchment simulation model that predicted streamflow and water chemistry by connecting a model of soil water balance to two groundwater reservoirs.
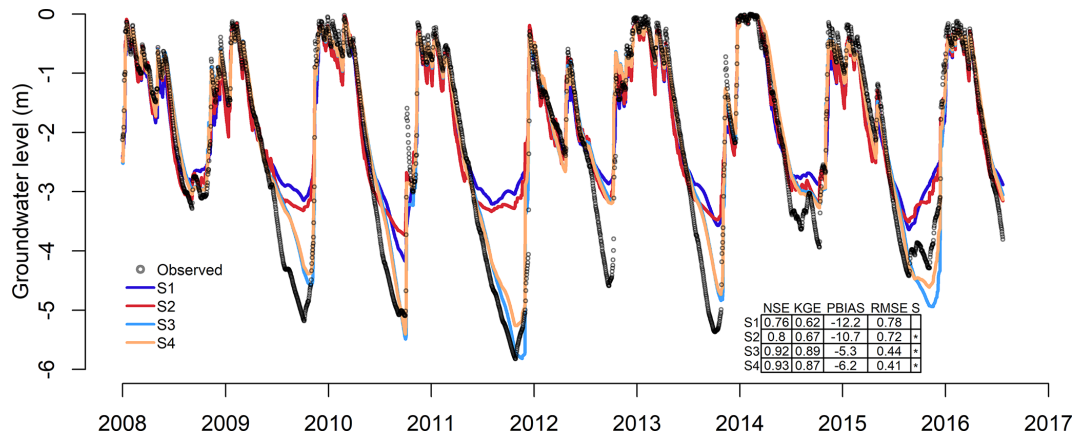
Figure 9. Observed and simulated groundwater levels for the four scenarios: S1 (streamflow only), S2 (streamflow + DOC), S3 (stream-flow + NO_3^-) and S4 (streamflow + DOC + NO_3^-). NSE – Nash–Sutcliffe model efficiency coefficient, KGE – Kling–Gupta efficiency, PBIAS – percent bias, RMSE – root-mean-square error, S – significance level. An asterisk in the significance level column indicates values that differed significantly ($p < 0.05$) from those for scenario S1 (two-sided Mann–Whitney test). See Table 3 for definitions of the performance metrics.

They found that calibrating the model using daily streamflow and monthly NO_3^- data simultaneously from a small lowland milk-production-oriented catchment improved hydrological understanding and estimated catchment NO_3^- flows relatively well. In particular, they were able to infer daily contributions of near-surface water; fast shallow groundwater; and slower, deeper groundwater to water and NO_3^- discharge. However, including NO_3^- data in the calibration overpredicted low flows compared to calibration using streamflow data alone. Yen et al. (2014) used regional estimates of annual denitrification mass and the percentage of NO_3^- load at the catchment outlet that had come from groundwater as soft data to constrain water-flow partitioning, which yielded realistic internal catchment behaviour but decreased the accuracy of predicted streamflow. In this study, when considering only the best-compromise model for each scenario, the use of solute data improved the representation of groundwater storage (S2, S3 and S4, Fig. 9) and soil moisture in the upslope zone (S2, Fig. 10b) but slightly decreased the accuracy of predicted streamflow in both calibration and evaluation periods (Fig. 4). In contrast, considering all hydrological signatures for discharge obtained from the envelope, S3 improved the model's ability to reproduce streamflow characteristics, especially low flows (Fig. 7) and groundwater level (Fig. 9).

We included solutes (DOC and NO_3^-) that have opposite dynamics and whose conceptual models had been successfully tested in the literature (Birkel et al., 2014; Fovet et al., 2015b), with the aim of adding useful constraints to the hydrological modelling. However, none of the scenarios that included DOC and/or NO_3^- improved both the model's representation of streamflow dynamics and internal consistency in representing groundwater level and soil moisture in the riparian and upslope zones. Given the limits of this study, it

remains uncertain whether including solutes with streamflow in calibration only improved the representation of hydrological states and flows of specific reservoirs or also improved the model's overall internal consistency. The first limit came from comparing point-scale in situ observations to simulated soil moisture and groundwater levels that represented catchment-scale storage, as these observations may not have represented the actual dynamics of groundwater and soil storage. Furthermore, although the dynamics of DOC and NO_3^- concentrations in the stream were represented well, the conceptualization of biogeochemical processes and transport of these solutes may remain too simple to represent internal state variables and flows of solutes. The model represents the hydrological and biogeochemical processes that are assumed to dominate, and these assumptions are limited by incomplete knowledge. In addition, the representation of reactive solutes increased the number of parameters and the complexity of the model. Consequently, it would be interesting to compare this approach to the use of non-reactive solutes in calibration, such as natural tracers that are assumed to be conservative, including chloride (Cl^-) and stable isotopes of water (^{18}O and ^2H) (Kirchner et al., 2010), to assess whether the model can reproduce the dynamics of both soil moisture and groundwater better.

The factors that improve internal hydrological consistency when solute data are included are not well understood. Streamflow aggregates information from many catchment-scale processes, but this information is too ambiguous to determine the exact catchment configuration (Kuppel et al., 2018b) or flow pathways that produced the observed signal (Woodward et al., 2017). This is because streamflow aggregates downstream along a convergent network towards a single outlet, but the divergent nature of an upstream network makes it impossible to uniquely backtrack the loca-
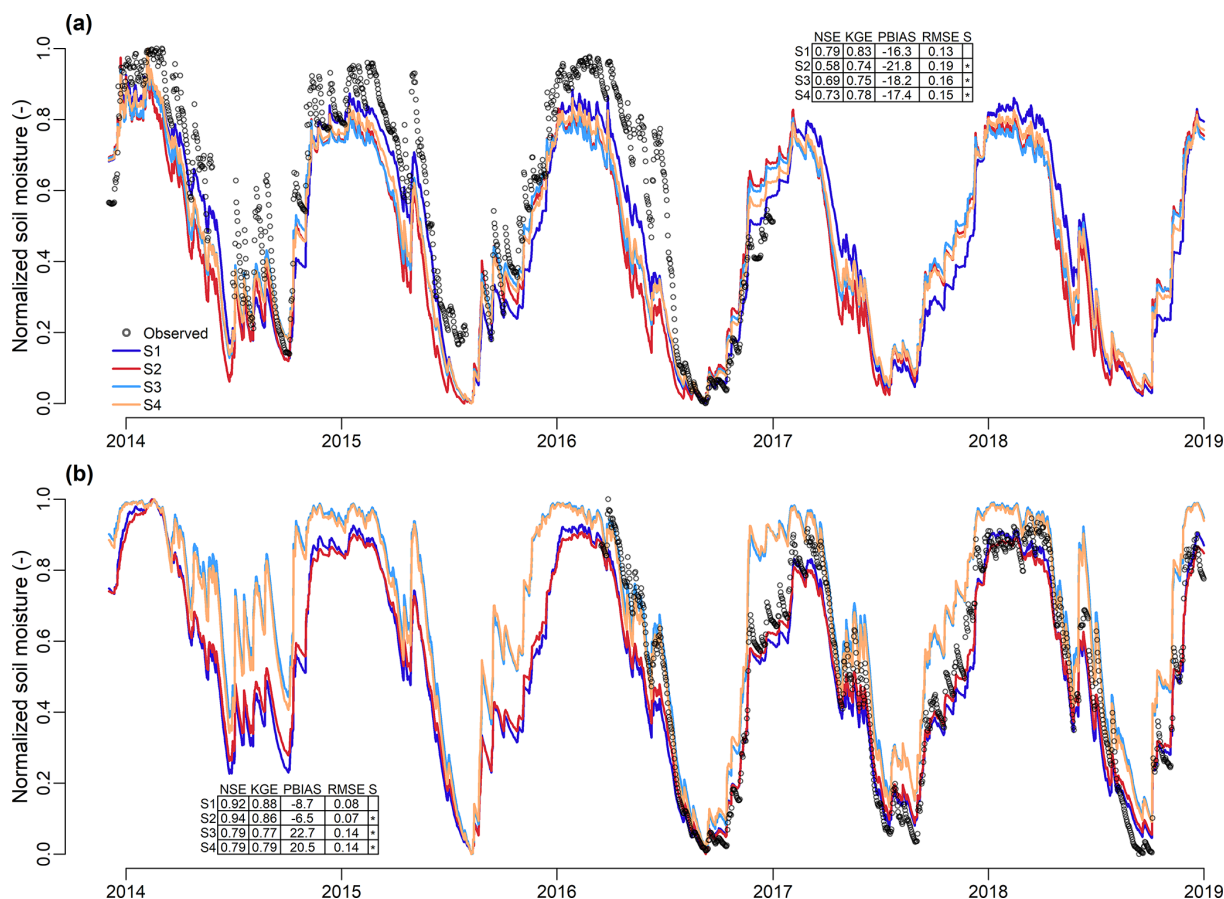
Figure 10. (a) Normalized observed (point PG2) and simulated soil moisture in the S_{UR} reservoir and **(b)** normalized observed (Toullo point) and simulated soil moisture in the S_U reservoir for four calibration scenarios: S1 (streamflow only), S2 (streamflow + DOC), S3 (streamflow + NO$_3^-$), and S4 (streamflow + DOC + NO$_3^-$). NSE – Nash–Sutcliffe model efficiency coefficient, KGE – Kling–Gupta efficiency, PBIAS – percent bias, RMSE: root-mean-square error, S – significance level. An asterisk in the significance level column indicates values that differed significantly ($p < 0.05$) from those for scenario S1 (two-sided Mann–Whitney test). See Table 3 for definitions of the performance metrics.

tions where the flow was generated (Kirchner et al., 2001). Thus, streamflow can be simulated well with many alternative model parameterizations, whether or not they are physically consistent (Kirchner, 2006). Results of the present study thus suggest that if streamflow alone is used for calibration, the model predicts discharge correctly for the wrong reason, as internal consistency, especially the representation of groundwater level, is not guaranteed. The model thus simulates water pathways and storage dynamics that do not represent those in the actual catchment. Consequently, it appears that the hydrological behaviour of the catchment required to reproduce the observed DOC and NO$_3^-$ concentrations in the stream is different from that required to reproduce only the observed discharge. This hypothesis is supported by the fact that the calibration scenarios influenced the main components of the water balance differently. For example, S3 yielded better representation of the groundwater reservoir, with good reproduction of the groundwater level

(Fig. 9) but lower evapotranspiration and higher water loss from the S_U reservoir than S1 (Fig. 11b). In comparison, S2 yielded better representation of upslope soil water storage (Fig. 10b) and a higher contribution of S_S to discharge than S1 (Fig. 11a). The large amount of information in the solute time series thus constrained internal reservoirs and water flows more than a streamflow-only approach, which increased internal consistency of the hydrological model. This occurs because a hydrological model only needs to represent an input–output response, whereas when biogeochemistry is included, a model needs to represent both residence-time distributions and biogeochemical processing to reproduce the observed stream concentrations (Medici et al., 2012) and the decrease in solute-input signals. The use of solute time series, which mitigates the equifinality problem, thus excluded infeasible model configurations that would have also yielded high performance (Dimitrova-Petrova et al., 2020; Kuppel et al., 2018b; Yen et al., 2014).
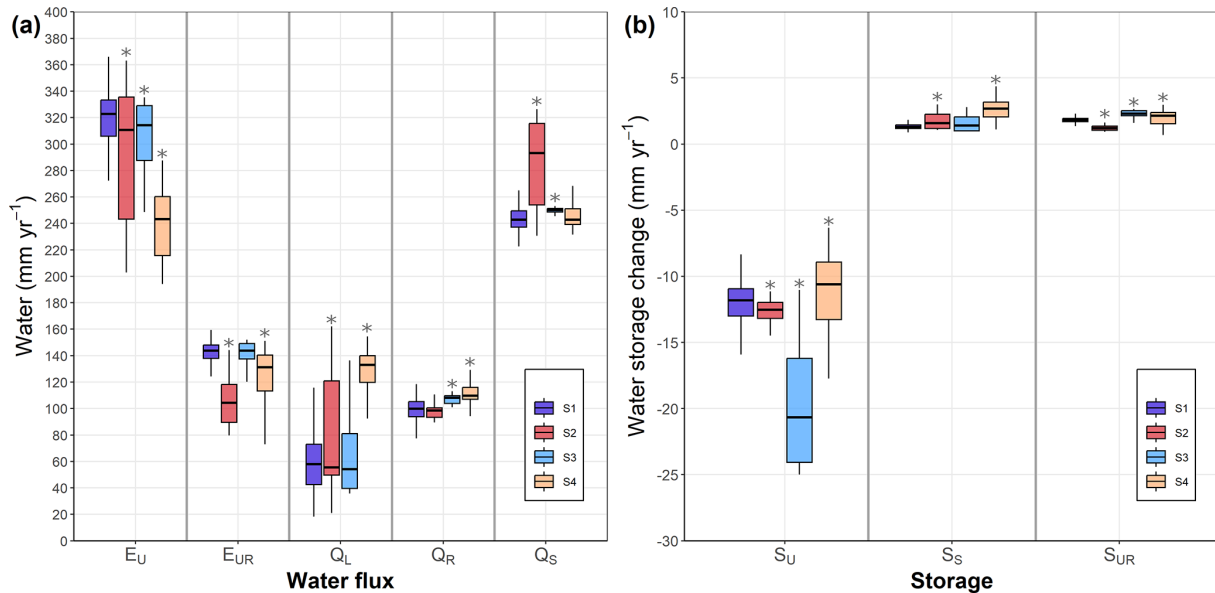
Figure 11. (a) Box plots of simulated annual water budgets for all Pareto fronts of each scenario (S1–S4) during the calibration and evaluation periods combined (1 August 2008–1 September 2016). **(b)** Box plots of changes in simulated storage of the main reservoirs of the model for all Pareto fronts of each scenario during the period. Whiskers represent 1.5 times the interquartile range. An asterisk above a box plot indicates values that differed significantly ($p < 0.05$) from those for scenario S1 (two-sided Mann–Whitney test).

An additional step is needed to understand the benefits of including solute data for internal hydrological consistency by analysing effects of including DOC and NO_3^- concentration data on the storage dynamics (state and flows) of model components. For example, the simulations showed that including NO_3^- data decreased k_S and S_{S_mix} (Fig. 8g and h), suggesting that simulations of NO_3^- dynamics were optimized at a lower groundwater mixing volume and lower flow rate in S_S. However, it is important to go further to understand why including NO_3^- concentration data improved simulation of groundwater level (Fig. 9) and low flow (Fig. 7). In this landscape, most of the NO_3^- leached from the unsaturated reservoir accumulates in the shallow groundwater (Aubert et al., 2013; Strohmenger et al., 2020). The groundwater, with a legacy mass storage of NO_3^- (Basu et al., 2010; Molenat et al., 2008), thus contributes water to the stream that sustains the base flow and export of NO_3^- (Aubert et al., 2013; Molenat et al., 2008). Given these characteristics, good reproduction of NO_3^- concentrations and flows in the stream, mainly supplied by groundwater, can be assumed to constrain the model sufficiently to yield good reproduction of water flows from the groundwater to the stream and thus good representation of groundwater level.

4.2   Effects on parameter uncertainties

Using a parsimonious hydrochemical model without explicit biogeochemical processes, Strohmenger et al. (2021) found that overall parameter uncertainties were higher when calibrating using solute data (DOC, NO_3^-) along with streamflow

data than when calibrating using streamflow data alone. They assumed that DOC and NO_3^- sources behave as infinite pools with a fixed concentration in each reservoir contributing to the stream. The modelling approach in the present study was relatively similar but explicitly represented biochemical processes related to DOC and NO_3^-. This approach resulted in decreased parameter uncertainty when solute concentrations were included in calibration, except for storage coefficients of the fast (k_F) and slow reservoirs (k_S) (Fig. 8). Comparing the results of these two studies suggests that the infinite-solute-pool assumption is sufficient to reproduce annual and storm-event dynamics of discharge and DOC and NO_3^- concentrations in the stream but is insufficient in calibration to constrain the model to adequately reproduce water storage dynamics and flow paths and to reduce uncertainties in hydrological parameters. In the infinite-solute-pool assumption, hydrological parameters are indeed less sensitive to solute concentrations than they are in models that explicitly represent biogeochemical processes and dynamic solute concentrations in reservoirs. Notably, the results of this study highlight that S4, which considered all constraints (i.e. streamflow and DOC and NO_3^- concentrations), greatly influenced the distributions of the most influential hydrological parameters, specifically Q_L and C_P, whose values were among the highest or lowest, respectively (Fig. 8b and j), and reproduced groundwater levels the best (Fig. 9). This highlights the importance of parameters Q_L and C_P, which determine inter-catchment groundwater flows and the recharge from S_U to S_S and S_{UR} to S_R, respectively, in ensuring that the model reproduced the observed groundwater dynamics. Based on

these results, for the model to best reproduce the dynamics of streamflow, concentrations (DOC, NO_3^-), and groundwater, recharge should be decreased and inter-catchment groundwater flow should be increased to ca. $0.35\,\mathrm{mm\,d^{-1}}$ (best-compromise parameter value for S4, Fig. 8j). This value is consistent with the values found in modelling studies of a similar physiographic headwater catchment in Brittany (Fovet et al., 2015a; Hrachowitz et al., 2014).

The model conceptualizes biogeochemical processes for DOC and NO_3^- in a relatively simple way but has reduced the uncertainties of the parameters. An additional step in future studies will be to analyse whether more complex representation of biogeochemical processes in the model can further reduce uncertainties in hydrological parameters. Results of the present study are consistent with those of other studies, in which inclusion of additional variables in multiple-objective calibration generally reduced parameter uncertainty (Tong et al., 2021). For example, Yen et al. (2014) found that including data related to water quality yielded lower parameter uncertainties than calibration using streamflow alone, especially for hydrological parameters that strongly influence denitrification. Silvestro et al. (2015) demonstrated that the equifinality of soil parameters was reduced by including satellite-derived soil moisture when calibrating a process-based, spatially distributed hydrological model. Similarly, Rajib et al. (2016) found that including satellite-derived soil moisture, especially that in the rooting zone, reduced parameter uncertainties, particularly for parameters related to subsurface hydrological processes.

4.3 Comparability of point-scale in situ measurements to catchment-scale storage

A remaining issue is the limited comparability of point-scale in situ measurements and simulated soil moisture and groundwater level to catchment-scale storage. In situ volumetric soil moisture was calculated as the mean of several TDR probes, which reduces uncertainty at the point scale, but upscaling these point measurements to a reservoir that represents a hillslope or riparian zone is associated with uncertainties. Consequently, we considered normalized soil moisture as a proxy for dynamics of unsaturated storage in hillslope and riparian zones. Similarly, we used the daily mean normalized water level at point PG5 as a proxy for groundwater storage dynamics. An additional step in future studies will be to determine how point measurements can be upscaled to areal-mean point-scale soil moisture and groundwater measurements compatible with catchment-scale storage. A complementary approach is to include other promising methods, such as remote sensing, to estimate the spatial distribution of storage in catchments, especially of soil moisture (Duethmann et al., 2022; Tong et al., 2021). The high spatial resolution, worldwide spatial coverage, and increasing availability of remotely sensed data may provide ample opportunities to further constrain hydrological models and their parame-

ters (Bouaziz et al., 2021; Duethmann et al., 2022; Gomis-Cebolla et al., 2022; Nijzink et al., 2018; Tong et al., 2021). Recent soil moisture data from satellite-derived soil-moisture products (e.g. SMAPL3E, SCATSAR, ASCAT DIREX SWI) with high spatial and temporal resolutions (e.g. 0.5–$9.0\,\mathrm{km}$ and 1–$3\,\mathrm{d}$, respectively) (Duethmann et al., 2022) would help constrain the model of the Kervidy–Naizin catchment. Other promising methods include cosmic-ray neutron-sensor probes to estimate dynamics of near-surface soil water storage (Dimitrova-Petrova et al., 2020) and geodesy and geophysical methods (Fovet et al., 2015a). Additional data can be used to assess the internal representation of evapotranspiration, which has a wide spatial and temporal distribution at the catchment scale, to provide more confidence in simulation of the partitioning of water between soil storage and groundwater recharge (Moazenzadeh and Izady, 2022). For example, using spatially and temporally gridded remotely sensed evapotranspiration data to calibrate the Soil and Water Assessment Tool (SWAT) hydrological model decreased the equifinality of the calibrated parameters compared to calibration using only streamflow data (Shah et al., 2021). These results demonstrate the benefit of using increasingly available open-access remotely sensed evapotranspiration data to improve calibration of hydrological models. These methods provide a spatially aggregated overview of catchment water content and go beyond traditional methods of direct storage observations at the point scale that are limited to a single reservoir (Dimitrova-Petrova et al., 2020).

4.4 Implications

This study's results indicate that solute data are important for improving the internal consistency of hydrological models, which can help guide collection of field data and modelling (Stadnyk and Holmes, 2023). When collecting field data for model calibration, it may be important to collect solute data along with streamflow data. These data can then be used in a hydrological model to which simple representations of biogeochemical processes are added to improve the representation of internal behaviour of the catchment by calibrating streamflow and solutes simultaneously. The type of solute measured is also important, as calibration using NO_3^- improved the internal consistency of the groundwater reservoir, while that using DOC improved the internal consistency of soil water storage in the upslope zone. With the increasing availability of solute data from catchment monitoring, this approach provides an objective way to improve representation of complex hydrological systems when information about their internal functioning is insufficient. A catchment model that represents observed behaviour of the system more accurately can then be used with confidence when assessing scenarios, such as those of nutrient remediation or climate change. If the internal behaviour of the hydrological system is not represented correctly, predicting streamflow acceptably is pointless and perhaps counter-productive, leading to erro-

neous conclusions and potential mismanagement of catchment resources. For example, Yen et al. (2014) showed that a lack of constraints to realistically represent the internal functioning of a catchment can lead to misleading assessments of pollution-control scenarios, even when typical streamflow performance criteria are satisfied.

The ability to apply this modelling approach to other catchments with different physiography will depend on the model's ability to represent dominant sources and pathways of DOC and NO_3^- concentrations that differ from those of Kervidy–Naizin. To address this question, we analysed the response of stream water chemistry to changes in discharge observed in this catchment and how the model represents it. Changes in solute concentrations as a function of discharge (i.e. concentration–discharge (CQ) relationships) (Appendix B) provide insight into how catchments store and release water and solutes and can therefore be considered a "fingerprint" of catchment transport, mixing, and reaction processes (Godsey et al., 2009; Knapp et al., 2020). Long-term seasonal CQ slopes for NO_3^- in Kervidy–Naizin generally indicated a chemostatic NO_3^- export regime (Fig. B1a). Indeed, this pattern often emerges in catchments with a spatially uniform distribution of abundant solute sources, such as NO_3^- in agricultural areas, which leads to a relatively constant release of solutes to the stream network (Bieroza et al., 2018). In contrast, in the winter of a few years (2010, 2012 and 2014), the CQ slope indicates instead a slightly more chemodynamic export regime with a dilution pattern. Long-term seasonal CQ slopes for DOC indicate a chemodynamic export regime with an accretion pattern that changes to a chemostatic export regime in autumn (Fig. B1b). The model reproduced the differing export regime of each solute from 2008–2016 relatively well (Fig. B1). Model performance was slightly lower for DOC (RMSE = 0.13–0.27) than for NO_3^- (RMSE = 0.08–0.21). For a few years, the model did not represent the export regime accurately. The export regime for NO_3^- observed in winter 2008 and 2009 was chemostatic, but the model simulated a chemodynamic export regime with a dilution pattern. The export regime for DOC observed in autumn 2011 and 2014 and summer 2012 and 2014 was an chemostatic export regime, but the model simulated a more chemodynamic export regime with an accretion pattern. As the model simulated hydrological dynamics relatively well during these periods (Fig. 4), it was likely overpredicting DOC. Analysis of the CQ relationships observed and simulated in Kervidy–Naizin highlighted two important points: (i) each solute in this catchment did not have a single pattern but instead seasonal and interannual differences in export regimes, and (ii) the parsimonious solute-transport model was able to reproduce different export regimes. Thus, this modelling approach may be applicable, in particular due to its flexible structure, to headwater catchments, whose characteristics and export regimes differ from those of Kervidy–Naizin. Applying the model to catchments whose streams can be intermittent would first require

solving the methodological issue of high NO_3^- concentrations in summer, when no observed data are available, to prevent overpredicting concentrations and risk overestimating NO_3^- flows in summer. The model can also be adapted to represent catchments whose hydrological and biochemical patterns differ from those of Kervidy–Naizin, where most DOC accumulates in the soils of the riparian zone and NO_3^- accumulates in the groundwater. For example, the reservoirs in which DOC is produced or lost can be modified easily. In addition, more complex models of biogeochemical processes can also be considered. While we represented heterotrophic denitrification as a constant, dynamic equations (Heinen, 2006) could easily be incorporated to represent the seasonality of this process.

5   Conclusion

The model reasonably reproduced the dynamics of discharge and solute (DOC and NO_3^-) concentrations in the stream of the headwater catchment simultaneously for all scenarios. Model predictions based on independent data indicated that the model generally reproduced the dynamics of groundwater level and soil moisture in upslope and riparian zones for all scenarios. Given the performance of the best-compromise model for each scenario, the results of this study tend to reject the first hypothesis, as using daily stream DOC and NO_3^- concentrations along with streamflow data to calibrate the model did not improve the model's performance for simulated streamflow for the calibration or evaluation period compared to calibration with streamflow alone. In contrast, considering all hydrological signatures for discharge obtained from the envelope, the scenario that included NO_3^- along with streamflow improved the model's ability to reproduce streamflow, especially low flows. For the second hypothesis, including solute data along with streamflow data in a multi-objective calibration strategy significantly improved the representation of groundwater storage and soil moisture in the upslope zone. The improvement in the representation of groundwater level was significant and relatively large for all scenarios when using one or both solutes along with streamflow for calibration compared to using only streamflow. In contrast, the improvement in the representation of soil moisture in the upslope zone was significant but relatively small only when using DOC concentration along with streamflow for calibration compared to using only streamflow. None of the scenarios that included solutes improved both the model's representation of streamflow dynamics and internal consistency in representing groundwater level and soil moisture in the riparian and upslope zones. Based on these results, it remains uncertain whether including solutes with streamflow in calibration improved only the representation of hydrological states and flows of specific reservoirs or also improved the model's overall internal hydrological consistency. For the third hypothesis, explicitly modelling

biochemical processes for DOC and NO_3^- reduced the uncertainty in hydrological parameters, except the storage coefficients of the fast and slow reservoirs, compared to an approach in which sources of DOC and NO_3^- were treated as infinite pools with fixed concentrations. The simultaneous inclusion of daily in-stream DOC and NO_3^- concentrations in the calibration strategy influenced the distribution of the most influential hydrological parameters of the model. Differences among the calibration scenarios also influenced the main components of the water balance. Calibrating the model with streamflow and solute concentrations simultaneously reduced predictions of evapotranspiration. Compared to calibration using streamflow alone, the inclusion of DOC increased the predicted contribution of groundwater to discharge, while the inclusion of NO_3^- increased the predicted loss of water from the rooting-zone reservoir. This modelling study demonstrated that including the large amount of information in solute time series in hydrological models provided an objective way to improve the representation of complex hydrological systems for which information about internal functioning was insufficient.

Appendix A: Definitions of variables and relationship between observed and simulated streamflow

Table A1. Symbols and definitions of variables in the hydrological model.

| Symbol	Definition	Symbol	Definition
$C_{H,R}$	Hillslope runoff coefficient [–]	Q_T	Total outflow [$L\,T^{-1}$]
C_P	Preferential recharge coefficient [–]	R_F	Recharge of fast reservoir [$L\,T^{-1}$]
$C_{R,R}$	Riparian runoff coefficient [–]	R_{FR}	Recharge of S_{UR} from S_F [$L\,T^{-1}$]
E_A	Actual evaporation [$L\,T^{-1}$]	R_P	Preferential recharge of the slow reservoir [$L\,T^{-1}$]
E_P	Potential evaporation [$L\,T^{-1}$]	R_R	Recharge of the riparian-zone reservoir [$L\,T^{-1}$]
E_U	Transpiration from S_U [$L\,T^{-1}$]	R_{SR}	Recharge of S_{UR} from S_S [$L\,T^{-1}$]
E_{UR}	Transpiration from S_{UR} [$L\,T^{-1}$]	R_{SS}	Recharge of the slow reservoir [$L\,T^{-1}$]
f	Proportion of the catchment covered by the riparian zone [–]	R_U	Infiltration into the unsaturated reservoir [$L\,T^{-1}$]
f_{SUR}	Proportion of water flow from S_S that passes through S_{UR} [–]	S_F	Storage in the fast reservoir [L]
k_F	Storage coefficient of the fast reservoir [T^{-1}]	S_R	Storage in the riparian reservoir [L]
k_R	Storage coefficient of the riparian-zone reservoir [T^{-1}]	S_S	Storage in the slow reservoir [L]
k_S	Storage coefficient of the slow reservoir [T^{-1}]	S_{S_mix}	Groundwater mixing storage in the slow reservoir [L]
L_P	Transpiration threshold [–]	S_U	Unsaturated storage [L]
P	Rainfall [$L\,T^{-1}$]	S_{U_max}	Storage capacity of the hillslope unsaturated zone [L]
P_{max}	Percolation capacity [$L\,T^{-1}$]	S_{UR}	Unsaturated storage in the riparian zone [L]
Q_L	Deep infiltration loss [L^{-1}]	S_{UR_max}	Storage capacity in the riparian unsaturated zone [L]
Q_R	Runoff from the riparian-zone reservoir [$L\,T^{-1}$]	β_H	Hillslope coefficient [–]
Q_S	Runoff from the slow reservoir [$L\,T^{-1}$]	β_R	Riparian coefficient [–]
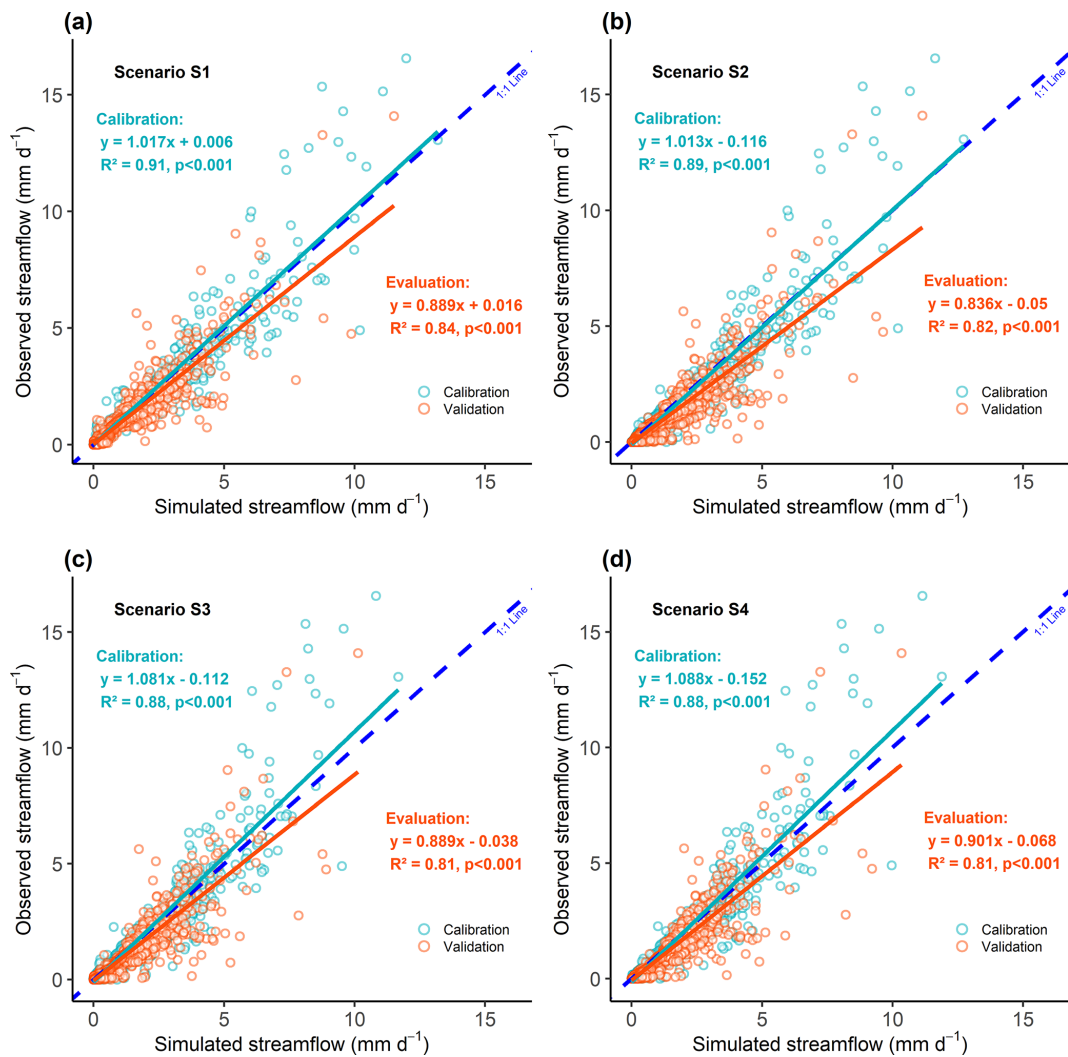
Figure A1. Relationship between observed and simulated streamflow for calibration and evaluation periods for four calibration scenarios: **(a)** S1 (streamflow only), **(b)** S2 (streamflow + DOC), **(c)** S3 (streamflow + NO_3^-), and **(d)** S4 (streamflow + DOC + NO_3^-). The dashed blue line is the 1 : 1 line. The light-green or orange lines are linear regressions for the calibration or evaluation period, respectively. All relationships were statistically significant ($p < 0.001$).

Appendix B: Concentration–discharge relationship

In general, the concentration–discharge (CQ) relationship allows three export regimes to be distinguished: (i) chemodynamic with an accretion pattern, (ii) chemodynamic with a dilution pattern, or (iii) chemostatic (Godsey et al., 2009; Musolff et al., 2017; Winter et al., 2021). "Chemodynamic" means that the variability in a solute's concentration is similar to or higher than that in Q, with concentrations either increasing (accretion) or decreasing (dilution) as Q increases (Winter et al., 2021). In contrast, chemostatic regimes have constant in-stream nutrient concentrations that are not significantly correlated with Q and have much lower variability (Bieroza et al., 2018). The slope of the linear relationship between $\ln(C)$ and $\ln(Q)$ (CQ slope) determines the export

regime: (i) chemodynamic with an accretion pattern when greater than 0.1, (ii) chemodynamic with a dilution pattern when less than -0.1, and (iii) chemostatic from -0.1 to 0.1 (Winter et al., 2021). The thresholds of -0.1 and 0.1 for the chemostatic regime were chosen according to Bieroza et al. (2018) and Winter et al. (2021).
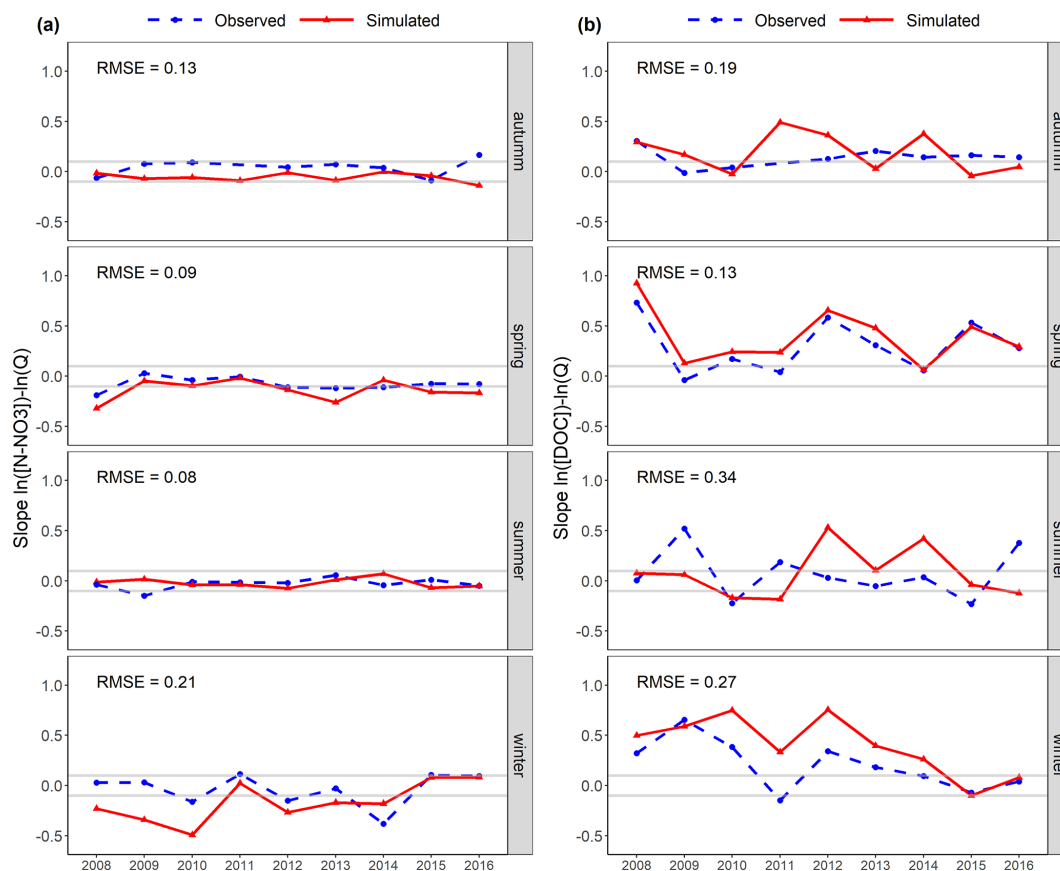
Figure B1. (a) Slope $\ln([N-NO_3]) - \ln(Q)$ for simulated nitrate (NO_3^-) data from scenario S3 (streamflow and stream NO_3^- concentration used for calibration). **(b)** Slope $\ln([DOC]) - \ln(Q)$ for simulated DOC data from scenario S2 (streamflow and stream DOC concentration used for calibration). Horizontal grey lines identify the boundary between a chemodynamic regime with a dilution pattern and a chemostatic regime (-0.1) and that between a chemostatic regime and a chemodynamic regime with an accretion pattern (0.1). RMSE: root-mean-square error.

References

Adeyeri, O. E., Laux, P., Arnault, J., Lawin, A. E., and Kunstmann, H.: Conceptual hydrological model calibration using multi-objective optimization techniques over the transboundary Komadugu-Yobe basin, Lake Chad Area, West Africa, J. Hydrol.: Reg. Stud., 27, 100655, https://doi.org/10.1016/j.ejrh.2019.100655, 2020.

Anderson, T. R., Groffman, P. M., Kaushal, S. S., and Walter, M. T.: Shallow Groundwater Denitrification in Riparian Zones of a Headwater Agricultural Landscape, J. Environ. Qual., 43, 732–744, https://doi.org/10.2134/jeq2013.07.0303, 2014.

Aubert, A. H., Gascuel-Odoux, C., Gruau, G., Akkal, N., Faucheux, M., Fauvel, Y., Grimaldi, C., Hamon, Y., Jaffrézic, A., Lecoz-Boutnik, M., Molénat, J., Petitjean, P., Ruiz, L., and Merot, P.: Solute transport dynamics in small, shallow groundwater-dominated agricultural catchments: insights from a high-frequency, multisolute 10 yr-long monitoring study, Hydrol. Earth Syst. Sci., 17, 1379–1391, https://doi.org/10.5194/hess-17-1379-2013, 2013.

Barton, L., McLay, C. D. A., Schipper, L. A., and Smith, C. T.: Annual denitrification rates in agricultural and forest soils: a review, Aust. J. Soil Res., 37, 1073–1073, 1999.

Basu, N. B., Destouni, G., Jawitz, J. W., Thompson, S. E., Loukinova, N. V., Darracq, A., Zanardo, S., Yaeger, M., Sivapalan, M., Rinaldo, A., and Rao, P. S. C.: Nutrient loads exported from managed catchments reveal emergent biogeochemical stationarity, Geophys. Res. Lett., 37, L23404, https://doi.org/10.1029/2010GL045168, 2010.

Benettin, P., van der Velde, Y., van der Zee, S. E. A. T. M., Rinaldo, A., and Botter, G.: Chloride circulation in a lowland catchment and the formulation of transport by travel time distributions, Water Resour. Res., 49, 4619–4632, https://doi.org/10.1002/wrcr.20309, 2013.

Benettin, P., Rodriguez, N. B., Sprenger, M., Kim, M., Klaus, J., Harman, C. J., van der Velde, Y., Hrachowitz, M., Botter, G., McGuire, K. J., Kirchner, J. W., Rinaldo, A., and McDonnell, J. J.: Transit Time Estimation in Catchments: Recent Developments and Future Directions, Water Resour. Res., 58, e2022WR033096, https://doi.org/10.1029/2022WR033096, 2022.

Bennett, K. E., Cherry, J. E., Balk, B., and Lindsey, S.: Using MODIS estimates of fractional snow cover area to improve streamflow forecasts in interior Alaska, Hydrol. Earth Syst. Sci., 23, 2439–2459, https://doi.org/10.5194/hess-23-2439-2019, 2019.

Benoit, M. and Veysset, P.: Calcul des Unités Gros Bétails: proposition d'une méthode basée sur les besoins énergétiques pour affiner l'étude des systèmes d'élevage, INRAE Productions Animales, 34, 139–160, https://doi.org/10.20870/productions-animales.2021.34.2.4855, 2021.

Beven, K.: On hypothesis testing in hydrology, Hydrol. Process., 15, 1655–1657, https://doi.org/10.1002/hyp.436, 2001.

Beven, K.: A manifesto for the equifinality thesis, J. Hydrol., 320, 18–36, https://doi.org/10.1016/j.jhydrol.2005.07.007, 2006.

Beven, K.: So how much of your error is epistemic? Lessons from Japan and Italy, Hydrol. Process., 27, 1677–1680, https://doi.org/10.1002/hyp.9648, 2013.

Beven, K. and Westerberg, I.: On red herrings and real herrings: disinformation and information in hydrological inference, Hydrol. Process., 25, 1676–1680, https://doi.org/10.1002/hyp.7963, 2011.

Beven, K. J.: Rainfall-runoff modelling: the primer, in: 2nd Edn., Wiley-Blackwell, Chichester, West Sussex, Hoboken, NJ, 457 pp., ISBN 80470714591, 2012.

Bieroza, M. Z., Heathwaite, A. L., Bechmann, M., Kyllmar, K., and Jordan, P.: The concentration-discharge slope as a tool for water quality management, Sci. Total Environ., 630, 738–749, https://doi.org/10.1016/j.scitotenv.2018.02.256, 2018.

Birkel, C. and Soulsby, C.: Linking tracers, water age and conceptual models to identify dominant runoff processes in a sparsely monitored humid tropical catchment, Hydrol. Process., 30, 4477–4493, https://doi.org/10.1002/hyp.10941, 2016.

Birkel, C., Tetzlaff, D., Dunn, S. M., and Soulsby, C.: Using time domain and geographic source tracers to conceptualize streamflow generation processes in lumped rainfall-runoff models: Dual-Tracer Conceptualized Streamflow Generation, Water Resour. Res., 47, W02515, https://doi.org/10.1029/2010WR009547, 2011.

Birkel, C., Soulsby, C., and Tetzlaff, D.: Integrating parsimonious models of hydrological connectivity and soil biogeochemistry to simulate stream DOC dynamics: Parsimonious Coupled DOC Model, J. Geophys. Res.-Biogeo., 119, 1030–1047, https://doi.org/10.1002/2013JG002551, 2014.

Birkel, C., Soulsby, C., and Tetzlaff, D.: Conceptual modelling to assess how the interplay of hydrological connectivity, catchment storage and tracer dynamics controls nonstationary water age estimates, Hydrol. Process., 29, 2956–2969, https://doi.org/10.1002/hyp.10414, 2015.

Birkel, C., Broder, T., and Biester, H.: Nonlinear and threshold-dominated runoff generation controls DOC export in a small peat catchment: Nonlinear Flow Paths Control DOC Export, J. Geophys. Res.-Biogeo., 122, 498–513, https://doi.org/10.1002/2016JG003621, 2017.

Birkel, C., Duvert, C., Correa, A., Munksgaard, N. C., Maher, D. T., and Hutley, L. B.: Tracer-Aided Modeling in the Low-Relief, Wet-Dry Tropics Suggests Water Ages and DOC Export Are Driven by Seasonal Wetlands and Deep Groundwater, Water Resour. Res., 56, e2019WR026175, https://doi.org/10.1029/2019WR026175, 2020.

Blazkova, S., Beven, K. J., and Kulasova, A.: On constraining TOPMODEL hydrograph simulations using partial saturated area information, Hydrol. Process., 16, 441–458, https://doi.org/10.1002/hyp.331, 2002.

Blöschl, G.: Scaling in hydrology: Invited Commentary, Hydrol. Process., 15, 709–711, https://doi.org/10.1002/hyp.432, 2001.

Böhlke, J. K., Antweiler, R. C., Harvey, J. W., Laursen, A. E., Smith, L. K., Smith, R. L., and Voytek, M. A.: Multi-scale measurements and modeling of denitrification in streams with varying flow and nitrate concentration in the upper Mississippi River basin, USA, Biogeochemistry, 93, 117–141, https://doi.org/10.1007/s10533-008-9282-8, 2009.

Botter, G., Bertuzzo, E., and Rinaldo, A.: Catchment residence and travel time distributions: The master equation: Catchment Residence Times, Geophys. Res. Lett., 38, L11403, https://doi.org/10.1029/2011GL047666, 2011.

Bouaziz, L., Weerts, A., Schellekens, J., Sprokkereef, E., Stam, J., Savenije, H., and Hrachowitz, M.: Redressing the balance: quantifying net intercatchment groundwater flows, Hydrol. Earth Syst. Sci., 22, 6415–6434, https://doi.org/10.5194/hess-22-6415-2018, 2018.

Bouaziz, L. J. E., Fenicia, F., Thirel, G., de Boer-Euser, T., Buitink, J., Brauer, C. C., De Niel, J., Dewals, B. J., Drogue, G., Grelier, B., Melsen, L. A., Moustakas, S., Nossent, J., Pereira, F., Sprokkereef, E., Stam, J., Weerts, A. H., Willems, P., Savenije, H. H. G., and Hrachowitz, M.: Behind the scenes of streamflow model performance, Hydrol. Earth Syst. Sci., 25, 1069–1095, https://doi.org/10.5194/hess-25-1069-2021, 2021.

Brocca, L., Melone, F., Moramarco, T., Wagner, W., and Hasenauer, S.: ASCAT soil wetness index validation through in situ and modeled soil moisture data in central Italy, Remote Sens. Environ., 114, 2745–2755, https://doi.org/10.1016/j.rse.2010.06.009, 2010.

Capell, R., Tetzlaff, D., and Soulsby, C.: Can time domain and source area tracers reduce uncertainty in rainfall-runoff models in larger heterogeneous catchments?, Water Resour. Res., 48, 2011WR011543, https://doi.org/10.1029/2011WR011543, 2012.

Carluer, N.: Vers une modélisation hydrologique adaptée à l'évaluation des pollutions diffuses: prise en compte du réseau anthropique. Adaptation au bassin versant de Naizin (Morbihan), PhD thesis, Doctorat Sciences de la terre, Université Pierre et Marie Curie Paris, https://hal.inrae.fr/tel-02577946v1 (last access: 19 December 2024), 1998.

Casal, L.: Evaluation de scénarios de gestion paysagère de l'azote par modélisation en bassins versants agricoles, These de doctorat, Rennes, Agrocampus Ouest, https://theses.fr/2018NSARD085 (last access: 19 December 2024), 2018.

Casal, L., Durand, P., Akkal-Corfini, N., Benhamou, C., Laurent, F., Salmon-Monviola, J., and Vertès, F.: Optimal location of set-aside areas to reduce nitrogen pollution: a modelling study, J. Agricult. Sci., 156, 1090–1102, https://doi.org/10.1017/S0021859618001144, 2018.

Casal, L., Durand, P., Akkal-Corfini, N., Benhamou, C., Laurent, F., Salmon-Monviola, J., Ferrant, S., Probst, A., Probst, J.-L., and Vertès, F.: Reduction of stream nitrate concentrations by land management in contrasted landscapes, Nutr. Cycl. Agroecosyst., 114, 1–17, https://doi.org/10.1007/s10705-019-09985-0, 2019.

Clark, M. P., Kavetski, D., and Fenicia, F.: Pursuing the method of multiple working hypotheses for hydrological modeling: Hypothesis Testing In Hydrology, Water Resour. Res., 47, W09301, https://doi.org/10.1029/2010WR009827, 2011.

Clark, M. P., Schaefli, B., Schymanski, S. J., Samaniego, L., Luce, C. H., Jackson, B. M., Freer, J. E., Arnold, J. R., Moore, R. D., Istanbulluoglu, E., and Ceola, S.: Improving the theoretical underpinnings of process-based hydrologic models, Water Resour. Res., 52, 2350–2365, https://doi.org/10.1002/2015WR017910, 2016.

Creed, I. F., McKnight, D. M., Pellerin, B. A., Green, M. B., Bergamaschi, B. A., Aiken, G. R., Burns, D. A., Findlay, S. E. G., Shanley, J. B., Striegl, R. G., Aulenbach, B. T., Clow, D. W., Laudon, H., McGlynn, B. L., McGuire, K. J., Smith, R. A., and Stackpoole, S. M.: The river as a chemostat: fresh perspectives on dissolved organic matter flowing down the river continuum, Can. J. Fish. Aquat. Sci., 72, 1272–1285, https://doi.org/10.1139/cjfas-2014-0400, 2015.

Criss, R. E. and Winston, W. E.: Do Nash values have value? Discussion and alternate proposals, Hydrol. Process., 22, 2723–2725, https://doi.org/10.1002/hyp.7072, 2008.

Dalzell, B. J., Filley, T. R., and Harbor, J. M.: The role of hydrology in annual organic carbon loads and terrestrial organic matter export from a midwestern agricultural watershed, Geochim. Cosmochim. Ac., 71, 1448–1462, https://doi.org/10.1016/j.gca.2006.12.009, 2007.

Delannoy, D., Maury, O., and Décome, J.: CLIMATIK: système d'information pour les données du réseau agroclimatique INRAE, V1, Recherche Data Gouv [data set], https://doi.org/10.57745/AJNXEN, 2022.

Demirel, M. C., Mai, J., Mendiguren, G., Koch, J., Samaniego, L., and Stisen, S.: Combining satellite data and appropriate objective functions for improved spatial pattern performance of a distributed hydrologic model, Hydrol. Earth Syst. Sci., 22, 1299–1315, https://doi.org/10.5194/hess-22-1299-2018, 2018.

Di Grazia, F., Garcia, X., Acuña, V., Llanos-Paez, O., Galgani, L., Gumiero, B., and Loiselle, S. A.: Modeling dissolved and particulate organic carbon dynamics at basin and sub-basin scales, Sci. Total Environ., 884, 163840, https://doi.org/10.1016/j.scitotenv.2023.163840, 2023.

Dimitrova-Petrova, K., Geris, J., Wilkinson, M. E., Rosolem, R., Verrot, L., Lilly, A., and Soulsby, C.: Opportunities and challenges in using catchment-scale storage estimates from cosmic ray neutron sensors for rainfall-runoff modelling, J. Hydrol., 586, 124878, https://doi.org/10.1016/j.jhydrol.2020.124878, 2020.

Duethmann, D., Smith, A., Soulsby, C., Kleine, L., Wagner, W., Hahn, S., and Tetzlaff, D.: Evaluating satellite-derived soil moisture data for improving the internal consistency of process-based ecohydrological modelling, J. Hydrol., 614, 128462, https://doi.org/10.1016/j.jhydrol.2022.128462, 2022.

Dupas, R., Ehrhardt, S., Musolff, A., Fovet, O., and Durand, P.: Long-term nitrogen retention and transit time distribution in agricultural catchments in western France, Environ. Res. Lett., 15, 115011, https://doi.org/10.1088/1748-9326/abbe47, 2020.

Eder, A., Weigelhofer, G., Pucher, M., Tiefenbacher, A., Strauss, P., Brandl, M., and Blöschl, G.: Pathways and composition of dissolved organic carbon in a small agricultural catchment during base flow conditions, Ecohydrol. Hydrobiol., 22, 96–112, https://doi.org/10.1016/j.ecohyd.2021.07.012, 2022.

Efstratiadis, A. and Koutsoyiannis, D.: Fitting Hydrological Models on Multiple Responses Using the Multiobjective Evolutionary Annealing-Simplex Approach, in: Practical Hydroinformatics: Computational Intelligence and Technological Developments in

Water Applications, edited by: Abrahart, R. J., See, L. M., and Solomatine, D. P., Springer, Berlin, Heidelberg, 259–273, https://doi.org/10.1007/978-3-540-79881-1_19, 2008.

Efstratiadis, A. and Koutsoyiannis, D.: One decade of multi-objective calibration approaches in hydrological modelling: a review, Hydrolog. Sci. J., 55, 58–78, https://doi.org/10.1080/02626660903526292, 2010.

Euser, T., Winsemius, H. C., Hrachowitz, M., Fenicia, F., Uhlenbrook, S., and Savenije, H. H. G.: A framework to assess the realism of model structures using hydrological signatures, Hydrol. Earth Syst. Sci., 17, 1893–1912, https://doi.org/10.5194/hess-17-1893-2013, 2013.

Euser, T., Hrachowitz, M., Winsemius, H. C., and Savenije, H. H. G.: The effect of forcing and landscape distribution on performance and consistency of model structures: Distribution Of Forcing And Model Structures, Hydrol. Process., 29, 3727–3743, https://doi.org/10.1002/hyp.10445, 2015.

Fenicia, F., Savenije, H. H. G., Matgen, P., and Pfister, L.: Understanding catchment behavior through stepwise model concept improvement: Catchment Behavior Through Stepwise Model, Water Resour. Res., 44, W01402, https://doi.org/10.1029/2006WR005563, 2008.

Fenicia, F., Kavetski, D., Reichert, P., and Albert, C.: Signature-Domain Calibration of Hydrological Models Using Approximate Bayesian Computation: Empirical Analysis of Fundamental Properties, Water Resour. Res., 54, 3958–3987, https://doi.org/10.1002/2017WR021616, 2018.

Fovet, O., Ruiz, L., Hrachowitz, M., Faucheux, M., and Gascuel-Odoux, C.: Hydrological hysteresis and its value for assessing process consistency in catchment conceptual models, Hydrol. Earth Syst. Sci., 19, 105–123, https://doi.org/10.5194/hess-19-105-2015, 2015a.

Fovet, O., Ruiz, L., Faucheux, M., Molénat, J., Sekhar, M., Vertès, F., Aquilina, L., Gascuel-Odoux, C., and Durand, P.: Using long time series of agricultural-derived nitrates for estimating catchment transit times, J. Hydrol., 522, 603–617, https://doi.org/10.1016/j.jhydrol.2015.01.030, 2015b.

Fovet, O., Ruiz, L., Gruau, G., Akkal, N., Aquilina, L., Busnot, S., Dupas, R., Durand, P., Faucheux, M., Fauvel, Y., Fléchard, C., Gilliet, N., Grimaldi, C., Hamon, Y., Jaffrezic, A., Jeanneau, L., Labasque, T., Le Henaff, G., Mérot, P., Molénat, J., Petitjean, P., Pierson-Wickmann, A., Squividant, H., Viaud, V., Walter, C., and Gascuel-Odoux, C.: AgrHyS: An Observatory of Response Times in Agro-Hydro Systems, Vadose Zone J., 17, 1–16, https://doi.org/10.2136/vzj2018.04.0066 2018.

Fovet, O., Cooper, D. M., Jones, D. L., Jones, T. G., and Evans, C. D.: Dynamics of dissolved organic matter in headwaters: comparison of headwater streams with contrasting DOM and nutrient composition, Aquat. Sci., 82, 29, https://doi.org/10.1007/s00027-020-0704-6, 2020.

Franks, S. W., Gineste, P., Beven, K. J., and Merot, P.: On constraining the predictions of a distributed model: The incorporation of fuzzy estimates of saturated areas into the calibration process, Water Resour. Res., 34, 787–797, https://doi.org/10.1029/97WR03041, 1998.

Freer, J. E., McMillan, H., McDonnell, J. J., and Beven, K. J.: Constraining dynamic TOPMODEL responses for imprecise water table information using fuzzy rule

based performance measures, J. Hydrol., 291, 254–277, https://doi.org/10.1016/j.jhydrol.2003.12.037, 2004.

Gao, H., Ding, Y., Zhao, Q., Hrachowitz, M., and Savenije, H. H. G.: The importance of aspect for modelling the hydrological response in a glacier catchment in Central Asia, Hydrol. Process., 31, 2842–2859, https://doi.org/10.1002/hyp.11224, 2017.

Gharari, S., Hrachowitz, M., Fenicia, F., Gao, H., and Savenije, H. H. G.: Using expert knowledge to increase realism in environmental system models can dramatically reduce the need for calibration, Hydrol. Earth Syst. Sci., 18, 4839–4859, https://doi.org/10.5194/hess-18-4839-2014, 2014.

Giustolisi, O. and Simeone, V.: Optimal design of artificial neural networks by a multi-objective strategy: groundwater level predictions, Hydrolog. Sci. J., 51, 502–523, https://doi.org/10.1623/hysj.51.3.502, 2006.

Godsey, S. E., Kirchner, J. W., and Clow, D. W.: Concentration–discharge relationships reflect chemostatic characteristics of US catchments, Hydrol. Process., 23, 1844–1864, https://doi.org/10.1002/hyp.7315, 2009.

Gomis-Cebolla, J., Garcia-Arias, A., Perpinyà-Vallès, M., and Francés, F.: Evaluation of Sentinel-1, SMAP and SMOS surface soil moisture products for distributed eco-hydrological modelling in Mediterranean forest basins, J. Hydrol., 608, 127569, https://doi.org/10.1016/j.jhydrol.2022.127569, 2022.

Guillaume, J. H. A., Jakeman, J. D., Marsili-Libelli, S., Asher, M., Brunner, P., Croke, B., Hill, M. C., Jakeman, A. J., Keesman, K. J., Razavi, S., and Stigter, J. D.: Introductory overview of identifiability analysis: A guide to evaluating whether you have the right type of data for your modeling purpose, Environ. Model. Softw., 119, 418–432, https://doi.org/10.1016/j.envsoft.2019.07.007, 2019.

Güntner, A., Uhlenbrook, S., Seibert, J., and Leibundgut, C.: Multi-criterial validation of TOPMODEL in a mountainous catchment, Hydrol. Process., 13, 1603–1620, https://doi.org/10.1002/(SICI)1099-1085(19990815)13:11<1603::AID-HYP830>3.0.CO;2-K, 1999.

Gupta, H. V., Kling, H., Yilmaz, K. K., and Martinez, G. F.: Decomposition of the mean squared error and NSE performance criteria: Implications for improving hydrological modelling, J. Hydrol., 377, 80–91, https://doi.org/10.1016/j.jhydrol.2009.08.003, 2009.

Gupta, H. V., Clark, M. P., Vrugt, J. A., Abramowitz, G., and Ye, M.: Towards a comprehensive assessment of model structural adequacy: Assessment Of Model Structural Adequacy, Water Resour. Res., 48, W08301, https://doi.org/10.1029/2011WR011044, 2012.

Hartmann, A., Wagener, T., Rimmer, A., Lange, J., Brielmann, H., and Weiler, M.: Testing the realism of model structures to identify karst system processes using water quality and quantity signatures: Karst System Identification, Water Resour. Res., 49, 3345–3358, https://doi.org/10.1002/wrcr.20229, 2013.

Hartmann, G. and Bárdossy, A.: Investigation of the transferability of hydrological models and a method to improve model calibration, Adv. Geosci., 5, 83–87, https://doi.org/10.5194/adgeo-5-83-2005, 2005.

Heinen, M.: Simplified denitrification models: Overview and properties, Geoderma, 133, 444–463, https://doi.org/10.1016/j.geoderma.2005.06.010, 2006.

Houska, T., Kraft, P., Chamorro-Chavez, A., and Breuer, L.: SPOTting Model Parameters Using a Ready-

Made Python Package, PLoS ONE, 10, e0145180, https://doi.org/10.1371/journal.pone.0145180, 2015.

Hrachowitz, M. and Clark, M. P.: HESS Opinions: The complementary merits of competing modelling philosophies in hydrology, Hydrol. Earth Syst. Sci., 21, 3953–3973, https://doi.org/10.5194/hess-21-3953-2017, 2017.

Hrachowitz, M., Savenije, H., Bogaard, T. A., Tetzlaff, D., and Soulsby, C.: What can flux tracking teach us about water age distribution patterns and their temporal dynamics?, Hydrol. Earth Syst. Sci., 17, 533–564, https://doi.org/10.5194/hess-17-533-2013, 2013.

Hrachowitz, M., Fovet, O., Ruiz, L., Euser, T., Gharari, S., Nijzink, R., Freer, J., Savenije, H. H. G., and Gascuel-Odoux, C.: Process consistency in models: The importance of system signatures, expert knowledge, and process complexity, Water Resour. Res., 50, 7445–7469, https://doi.org/10.1002/2014WR015484, 2014.

Hrachowitz, M., Fovet, O., Ruiz, L., and Savenije, H. H. G.: Transit time distributions, legacy contamination and variability in biogeochemical $1/f^\alpha$ scaling: how are hydrological response dynamics linked to water quality at the catchment scale?: How are Hydrological Response Dynamics Linked to Water Quality?, Hydrol. Process., 29, 5241–5256, https://doi.org/10.1002/hyp.10546, 2015.

Hrachowitz, M., Benettin, P., van Breukelen, B. M., Fovet, O., Howden, N. J. K., Ruiz, L., van der Velde, Y., and Wade, A. J.: Transit times-the link between hydrology and water quality at the catchment scale: Linking hydrology and transit times, WIREs Water, 3, 629–657, https://doi.org/10.1002/wat2.1155, 2016.

Hrachowitz, M., Stockinger, M., Coenders-Gerrits, M., van der Ent, R., Bogena, H., Lücke, A., and Stumpp, C.: Reduction of vegetation-accessible water storage capacity after deforestation affects catchment travel time distributions and increases young water fractions in a headwater catchment, Hydrol. Earth Syst. Sci., 25, 4887–4915, https://doi.org/10.5194/hess-25-4887-2021, 2021.

Huang, Y. and Bardossy, A.: Impacts of Data Quantity and Quality on Model Calibration: Implications for Model Parameterization in Data-Scarce Catchments, Water, 12, 2352, https://doi.org/10.3390/w12092352, 2020.

Hulsman, P., Winsemius, H. C., Michailovsky, C. I., Savenije, H. H. G., and Hrachowitz, M.: Using altimetry observations combined with GRACE to select parameter sets of a hydrological model in a data-scarce region, Hydrol. Earth Syst. Sci., 24, 3331–3359, https://doi.org/10.5194/hess-24-3331-2020, 2020.

Humbert, G., Jaffrezic, A., Fovet, O., Gruau, G., and Durand, P.: Dry-season length and runoff control annual variability in stream DOC dynamics in a small, shallow groundwater-dominated agricultural watershed, Water Resour. Res., 51, 7860–7877, https://doi.org/10.1002/2015WR017336, 2015.

Inamdar, S. P. and Mitchell, M. J.: Hydrologic and topographic controls on storm-event exports of dissolved organic carbon (DOC) and nitrate across catchment scales, Water Resour. Res., 42, W03421, https://doi.org/10.1029/2005WR004212, 2006.

INRAE-AgrHyS: AgrHyS Observatory, https://agrhys.rennes.hub.inrae.fr/ (last access: 23 December 2024), 2024.

ISO 10304: Water Quality – Determination of Dissolved Anions by Liquid Chromatography of Ions – Part 1: Determination of Bromide, Chloride, Fluoride, Nitrate, Nitrite, Phosphate and Sulfate, 15 pp., https://www.iso.org/standard/46004.html (last access: 19 December 2024), 2007.

Jothityangkoon, C., Sivapalan, M., and Farmer, D. L.: Process controls of water balance variability in a large semi-arid catchment: downward approach to hydrological model development, J. Hydrol., 254, 174–198, https://doi.org/10.1016/S0022-1694(01)00496-6, 2001.

Kalbitz, K. and Kaiser, K.: Contribution of dissolved organic matter to carbon storage in forest mineral soils, J. Plant Nutr. Soil Sci., 171, 52–60, https://doi.org/10.1002/jpln.200700043, 2008.

Kavetski, D., Fenicia, F., Reichert, P., and Albert, C.: Signature-Domain Calibration of Hydrological Models Using Approximate Bayesian Computation: Theory and Comparison to Existing Applications, Water Resour. Res., 54, 4059–4083, https://doi.org/10.1002/2017WR020528, 2018.

Kirchner, J. W.: Getting the right answers for the right reasons: Linking measurements, analyses, and models to advance the science of hydrology: Getting The Right Answers For The Right Reasons, Water Resour. Res., 42, W03S04, https://doi.org/10.1029/2005WR004362, 2006.

Kirchner, J. W., Feng, X., and Neal, C.: Catchment-scale advection and dispersion as a mechanism for fractal scaling in stream tracer concentrations, J. Hydrol., 254, 82–101, https://doi.org/10.1016/S0022-1694(01)00487-5, 2001.

Kirchner, J. W., Tetzlaff, D., and Soulsby, C.: Comparing chloride and water isotopes as hydrological tracers in two Scottish catchments, Hydrol. Process., 24, 1631–1645, https://doi.org/10.1002/hyp.7676, 2010.

Knapp, J. L. A., von Freyberg, J., Studer, B., Kiewiet, L., and Kirchner, J. W.: Concentration–discharge relationships vary among hydrological events, reflecting differences in event characteristics, Hydrol. Earth Syst. Sci., 24, 2561–2576, https://doi.org/10.5194/hess-24-2561-2020, 2020.

Koch, J. C., Runkel, R. L., Striegl, R., and McKnight, D. M.: Hydrologic controls on the transport and cycling of carbon and nitrogen in a boreal catchment underlain by continuous permafrost, J. Geophys. Res.-Biogeo., 118, 698–712, https://doi.org/10.1002/jgrg.20058, 2013.

Köhler, S., Buffam, I., Jonsson, A., and Bishop, K.: Photochemical and microbial processing of stream and soil water dissolved organic matter in a boreal forested catchment in northern Sweden, Aquat. Sci., 64, 269–281, https://doi.org/10.1007/s00027-002-8071-z, 2002.

Kreye, P., Gelleszun, M., and Meon, G.: Parameter identification in hydrological models using groundwater-level measurements and satellite-based soil moisture, Hydrolog. Sci. J., 64, 633–652, https://doi.org/10.1080/02626667.2019.1599120, 2019.

Kunnath-Poovakka, A., Ryu, D., Renzullo, L. J., and George, B.: The efficacy of calibrating hydrologic model using remotely sensed evapotranspiration and soil moisture for streamflow prediction, J. Hydrol., 535, 509–524, https://doi.org/10.1016/j.jhydrol.2016.02.018, 2016.

Kuppel, S., Tetzlaff, D., Maneta, M. P., and Soulsby, C.: EcH$_2$O-iso 1.0: water isotopes and age tracking in a process-based, distributed ecohydrological model, Geosci. Model Dev., 11, 3045–3069, https://doi.org/10.5194/gmd-11-3045-2018, 2018a.

Kuppel, S., Tetzlaff, D., Maneta, M. P., and Soulsby, C.: What can we learn from multi-data calibration of a process-based eco-

hydrological model?, Environ. Model. Softw., 101, 301–316, https://doi.org/10.1016/j.envsoft.2018.01.001, 2018b.

Lambert, T., Pierson-Wickmann, A.-C., Gruau, G., Jaffrezic, A., Petitjean, P., Thibault, J.-N., and Jeanneau, L.: Hydrologically driven seasonal changes in the sources and production mechanisms of dissolved organic carbon in a small lowland catchment, Water Resour. Res., 49, 5792–5803, https://doi.org/10.1002/wrcr.20466, 2013.

Lambert, T., Pierson-Wickmann, A.-C., Gruau, G., Jaffrezic, A., Petitjean, P., Thibault, J. N., and Jeanneau, L.: DOC sources and DOC transport pathways in a small headwater catchment as revealed by carbon isotope fluctuation during storm events, Biogeosciences, 11, 3043–3056, https://doi.org/10.5194/bg-11-3043-2014, 2014.

Lan, T., Lin, K., Xu, C.-Y., Tan, X., and Chen, X.: Dynamics of hydrological-model parameters: mechanisms, problems and solutions, Hydrol. Earth Syst. Sci., 24, 1347–1366, https://doi.org/10.5194/hess-24-1347-2020, 2020.

Le Moine, N., Andréassian, V., Perrin, C., and Michel, C.: How can rainfall-runoff models handle intercatchment groundwater flows? Theoretical study based on 1040 French catchments, Water Resour. Res., 43, W06428, https://doi.org/10.1029/2006WR005608, 2007.

López López, P., Sutanudjaja, E. H., Schellekens, J., Sterk, G., and Bierkens, M. F. P.: Calibration of a large-scale hydrological model using satellite-based soil moisture and evapotranspiration products, Hydrol. Earth Syst. Sci., 21, 3125–3144, https://doi.org/10.5194/hess-21-3125-2017, 2017.

Matos-Moreira, M., Lemercier, B., Dupas, R., Michot, D., Viaud, V., Akkal-Corfini, N., Louis, B., and Gascuel-Odoux, C.: High-resolution mapping of soil phosphorus concentration in agricultural landscapes with readily available or detailed survey data, Eur. J. Soil Sci., 68, 281–294, https://doi.org/10.1111/ejss.12420, 2017.

McMillan, H., Tetzlaff, D., Clark, M., and Soulsby, C.: Do time-variable tracers aid the evaluation of hydrological model structure? A multimodel approach, Water Resour. Res., 48, W05501, https://doi.org/10.1029/2011WR011688, 2012.

Medici, C., Wade, A. J., and Francés, F.: Does increased hydrochemical model complexity decrease robustness?, J. Hydrol., 440–441, 1–13, https://doi.org/10.1016/j.jhydrol.2012.02.047, 2012.

Minville, M., Cartier, D., Guay, C., Leclaire, L.-A., Audet, C., Le Digabel, S., and Merleau, J.: Improving process representation in conceptual hydrological model calibration using climate simulations, Water Resour. Res., 50, 5044–5073, https://doi.org/10.1002/2013WR013857, 2014.

Moazenzadeh, R. and Izady, A.: A hybrid calibration method for improving hydrological systems using ground-based and remotely-sensed observations, J. Hydrol., 615, 128688, https://doi.org/10.1016/j.jhydrol.2022.128688, 2022.

Molenat, J., Gascuel, C., Davy, P., and Durand, P.: How to model shallow water-table depth variations: the case of the Kervidy-Naizin catchment – France, Hydrol. Process., 19, 901–920, https://doi.org/10.1002/hyp.5546, 2005.

Molenat, J., Gascuel-Odoux, C., Ruiz, L., and Gruau, G.: Role of water table dynamics on stream nitrate export and concentration in agricultural headwater catchment (France), J. Hydrol., 348, 363–378, https://doi.org/10.1016/j.jhydrol.2007.10.005, 2008.

Monteil, C., Zaoui, F., Le Moine, N., and Hendrickx, F.: Multi-objective calibration by combination of stochastic and gradient-like parameter generation rules – the caRamel algorithm, Hydrol. Earth Syst. Sci., 24, 3189–3209, https://doi.org/10.5194/hess-24-3189-2020, 2020.

Morel, B., Durand, P., Jaffrezic, A., Gruau, G., and Molenat, J.: Sources of dissolved organic carbon during stormflow in a headwater agricultural catchment, Hydrol. Process., 23, 2888–2901, https://doi.org/10.1002/hyp.7379, 2009.

Moriasi, D. N., Arnold, J. G., Van Liew, M. W., Bingner, R. L., Harmel, R. D., and Veith, T. L.: Model evaluation guidelines for systematic quantification of accuracy in watershed simulations, T. ASABE, 50, 885–900, https://doi.org/10.13031/2013.23153, 2007.

Mostafaie, A., Forootan, E., Safari, A., and Schumacher, M.: Comparing multi-objective optimization techniques to calibrate a conceptual hydrological model using in situ runoff and daily GRACE data, Comput. Geosci., 22, 789–814, https://doi.org/10.1007/s10596-018-9726-8, 2018.

Moussa, R., Chahinian, N., and Bocquillon, C.: Distributed hydrological modelling of a Mediterranean mountainous catchment – Model construction and multi-site validation, J. Hydrol., 337, 35–51, https://doi.org/10.1016/j.jhydrol.2007.01.028, 2007.

Musolff, A., Fleckenstein, J. H., Rao, P. S. C., and Jawitz, J. W.: Emergent archetype patterns of coupled hydrologic and biogeochemical responses in catchments: Emergence of Archetype $C–Q$ Patterns, Geophys. Res. Lett., 44, 4143–4151, https://doi.org/10.1002/2017GL072630, 2017.

Nash, J. E. and Sutcliffe, J. V.: River flow forecasting through conceptual models part I – A discussion of principles, J. Hydrol., 10, 282–290, https://doi.org/10.1016/0022-1694(70)90255-6, 1970.

Nijzink, R. C., Almeida, S., Pechlivanidis, I. G., Capell, R., Gustafssons, D., Arheimer, B., Parajka, J., Freer, J., Han, D., Wagener, T., van Nooijen, R. R. P., Savenije, H. H. G., and Hrachowitz, M.: Constraining Conceptual Hydrological Models With Multiple Information Sources, Water Resour. Res., 54, 8332–8362, https://doi.org/10.1029/2017WR021895, 2018.

Nossent, J., Elsen, P., and Bauwens, W.: Sobol' sensitivity analysis of a complex environmental model, Environ. Model. Softw., 26, 1515–1525, https://doi.org/10.1016/j.envsoft.2011.08.010, 2011.

OZCAR: AgrHys Observatory, https://www.ozcar-ri.org/agrhys-observatory/ (last access: 23 December 2024), 2024.

Pelletier, A. and Andréassian, V.: On constraining a lumped hydrological model with both piezometry and streamflow: results of a large sample evaluation, Hydrol. Earth Syst. Sci., 26, 2733–2758, https://doi.org/10.5194/hess-26-2733-2022, 2022.

Penman, H. L.: Estimating evaporation, Eos Trans. Am. Geophys. Union, 37, 43–50, https://doi.org/10.1029/TR037i001p00043, 1956.

Pesántez, J., Birkel, C., Mosquera, G. M., Célleri, R., Contreras, P., Cárdenas, I., and Crespo, P.: Bridging the gap from hydrological to biogeochemical processes using tracer-aided hydrological models in a tropical montane ecosystem, J. Hydrol., 619, 129328, https://doi.org/10.1016/j.jhydrol.2023.129328, 2023.

Pettersson, A., Arheimer, B., and Johansson, B.: Nitrogen Concentrations Simulated with HBV-N: New Response Function and Calibration Strategy, Hydrol. Res., 32, 227–248, https://doi.org/10.2166/nh.2001.0014, 2001.

Piovano, T. I., Tetzlaff, D., Carey, S. K., Shatilla, N. J., Smith, A., and Soulsby, C.: Spatially distributed tracer-aided runoff modelling and dynamics of storage and water ages in a permafrost-influenced catchment, Hydrol. Earth Syst. Sci., 23, 2507–2523, https://doi.org/10.5194/hess-23-2507-2019, 2019.

Rajat and Athira, P.: Calibration of hydrological models considering process interdependence: A case study of SWAT model, Environ. Model. Softw., 144, 105131, https://doi.org/10.1016/j.envsoft.2021.105131, 2021.

Rajib, M. A., Merwade, V., and Yu, Z.: Multi-objective calibration of a hydrologic model using spatially distributed remotely sensed/in-situ soil moisture, J. Hydrol., 536, 192–207, https://doi.org/10.1016/j.jhydrol.2016.02.037, 2016.

Rakovec, O., Kumar, R., Mai, J., Cuntz, M., Thober, S., Zink, M., Attinger, S., Schäfer, D., Schrön, M., and Samaniego, L.: Multiscale and Multivariate Evaluation of Water Fluxes and States over European River Basins, J. Hydrometeor., 17, 287–307, https://doi.org/10.1175/JHM-D-15-0054.1, 2016.

Raymond, P. A. and Saiers, J. E.: Event controlled DOC export from forested watersheds, Biogeochemistry, 100, 197–209, https://doi.org/10.1007/s10533-010-9416-7, 2010.

Reed, P. and Devireddy, V.: Groundwater monitoring design: a case study combining epsilon dominance archiving and automatic parameterization for the nsga-ii, in: Applications of Multi-Objective Evolutionary Algorithms, Volume 1, World Scientific, 79–100, https://doi.org/10.1142/9789812567796_0004, 2004.

Reusser, D. E., Buytaert, W., and Zehe, E.: Temporal dynamics of model parameter sensitivity for computationally expensive models with the Fourier amplitude sensitivity test: Temporal Dynamics Of Model Parameter Sensitivity, Water Resour. Res., 47, W07551, https://doi.org/10.1029/2010WR009947, 2011.

Riboust, P., Thirel, G., Moine, N. L., and Ribstein, P.: Revisiting a Simple Degree-Day Model for Integrating Satellite Data: Implementation of Swe-Sca Hystereses, J. Hydrol. Hydromech., 67, 70–81, https://doi.org/10.2478/johh-2018-0004, 2019.

Rinaldo, A., Benettin, P., Harman, C. J., Hrachowitz, M., McGuire, K. J., van der Velde, Y., Bertuzzo, E., and Botter, G.: Storage selection functions: A coherent framework for quantifying how catchments store and release water and solutes: On Storage Selection Functions, Water Resour. Res., 51, 4840–4847, https://doi.org/10.1002/2015WR017273, 2015.

Salmon-Monviola, J., Moreau, P., Benhamou, C., Durand, P., Merot, P., Oehler, F., and Gascuel-Odoux, C.: Effect of climate change and increased atmospheric CO_2 on hydrological and nitrogen cycling in an intensive agricultural headwater catchment in western France, Climatic Change, 120, 433–447, https://doi.org/10.1007/s10584-013-0828-y, 2013.

Salmon-Monviola, J., Fovet, O., and Hrachowitz, M.: Modeling water, and nitrate and dissolved organic carbon concentrations dynamics in an agricultural headwater catchment, Zenodo [code], https://doi.org/10.5281/zenodo.10161243, 2023.

Saltelli, A.: Making best use of model evaluations to compute sensitivity indices, Comput. Phys. Commun., 145, 280–297, https://doi.org/10.1016/S0010-4655(02)00280-1, 2002.

Saltelli, A., Chan, K., and Scott, E. M.: Sensitivity Analysis, 504 pp., ISBN 978-0-470-74382-9, https://www.wiley.com/en-us/Sensitivity+Analysis-p-9780470743829 (last access: 19 December 2024), 2009.

Saltelli, A. and Annoni, P.: How to avoid a perfunctory sensitivity analysis, Environ. Model. Softw., 25, 1508–1517, https://doi.org/10.1016/j.envsoft.2010.04.012, 2010.

Saltelli, A., Tarantola, S., and Chan, K. P.-S.: A Quantitative Model-Independent Method for Global Sensitivity Analysis of Model Output, Technometrics, 41, 39–56, https://doi.org/10.1080/00401706.1999.10485594, 1999.

Sawicz, K., Wagener, T., Sivapalan, M., Troch, P. A., and Carrillo, G.: Catchment classification: empirical analysis of hydrologic similarity based on catchment function in the eastern USA, Hydrol. Earth Syst. Sci., 15, 2895–2911, https://doi.org/10.5194/hess-15-2895-2011, 2011.

Seibert, J.: Multi-criteria calibration of a conceptual runoff model using a genetic algorithm, Hydrol. Earth Syst. Sci., 4, 215–224, https://doi.org/10.5194/hess-4-215-2000, 2000.

Seibert, J., Rodhe, A., and Bishop, K.: Simulating interactions between saturated and unsaturated storage in a conceptual runoff model, Hydrol. Process., 17, 379–390, https://doi.org/10.1002/hyp.1130, 2003.

Seibert, J., Grabs, T., Köhler, S., Laudon, H., Winterdahl, M., and Bishop, K.: Linking soil- and stream-water chemistry based on a Riparian Flow-Concentration Integration Model, Hydrol. Earth Syst. Sci., 13, 2287–2297, https://doi.org/10.5194/hess-13-2287-2009, 2009.

Shah, S., Duan, Z., Song, X., Li, R., Mao, H., Liu, J., Ma, T., and Wang, M.: Evaluating the added value of multi-variable calibration of SWAT with remotely sensed evapotranspiration data for improving hydrological modeling, J. Hydrol., 603, 127046, https://doi.org/10.1016/j.jhydrol.2021.127046, 2021.

Shang, P., Lu, Y., Du, Y., Jaffé, R., Findlay, R. H., and Wynn, A.: Climatic and watershed controls of dissolved organic matter variation in streams across a gradient of agricultural land use, Sci. Total Environ., 612, 1442–1453, https://doi.org/10.1016/j.scitotenv.2017.08.322, 2018.

Shin, M.-J. and Kim, C.-S.: Assessment of the suitability of rainfall–runoff models by coupling performance statistics and sensitivity analysis, Hydrol. Res., 48, 1192–1213, https://doi.org/10.2166/nh.2016.129, 2017.

Silvestro, F., Gabellani, S., Rudari, R., Delogu, F., Laiolo, P., and Boni, G.: Uncertainty reduction and parameter estimation of a distributed hydrological model with ground and remote-sensing data, Hydrol. Earth Syst. Sci., 19, 1727–1751, https://doi.org/10.5194/hess-19-1727-2015, 2015.

Song, X., Zhang, J., Zhan, C., Xuan, Y., Ye, M., and Xu, C.: Global sensitivity analysis in hydrological modeling: Review of concepts, methods, theoretical framework, and applications, J. Hydrol., 523, 739–757, https://doi.org/10.1016/j.jhydrol.2015.02.013, 2015.

Sorel, L., Viaud, V., Durand, P., and Walter, C.: Modeling spatiotemporal crop allocation patterns by a stochastic decision tree method, considering agronomic driving factors, Agricult. Syst., 103, 647–655, https://doi.org/10.1016/j.agsy.2010.08.003, 2010.

Stadnyk, T. A. and Holmes, T. L.: Large scale hydrologic and tracer aided modelling: A review, J. Hydrol., 618, 129177, https://doi.org/10.1016/j.jhydrol.2023.129177, 2023.

Strohmenger, L., Fovet, O., Akkal-Corfini, N., Dupas, R., Durand, P., Faucheux, M., Gruau, G., Hamon, Y., Jaffrezic, A., Minaudo, C., Petitjean, P., and Gascuel-Odoux, C.: Multitemporal Relationships Between the Hydroclimate and Ex-

ports of Carbon, Nitrogen, and Phosphorus in a Small Agricultural Watershed, Water Resour. Res., 56, e2019WR026323, https://doi.org/10.1029/2019WR026323, 2020.

Strohmenger, L., Fovet, O., Hrachowitz, M., Salmon-Monviola, J., and Gascuel-Odoux, C.: Is a simple model based on two mixing reservoirs able to reproduce the intra-annual dynamics of DOC and NO_3 stream concentrations in an agricultural headwater catchment?, Sci. Total Environ., 794, 148715, https://doi.org/10.1016/j.scitotenv.2021.148715, 2021.

Sun, X., Croke, B., Jakeman, A., and Roberts, S.: Benchmarking Active Subspace methods of global sensitivity analysis against variance-based Sobol' and Morris methods with established test functions, Environ. Model. Softw., 149, 105310, https://doi.org/10.1016/j.envsoft.2022.105310, 2022.

Sutanudjaja, E. H., van Beek, L. P. H., de Jong, S. M., van Geer, F. C., and Bierkens, M. F. P.: Calibrating a large-extent high-resolution coupled groundwater-land surface model using soil moisture and discharge data: Calibrating Groundwater-Land Surface Model, Water Resour. Res., 50, 687–705, https://doi.org/10.1002/2013WR013807, 2014.

Taylor, P. G. and Townsend, A. R.: Stoichiometric control of organic carbon–nitrate relationships from soils to the sea, Nature, 464, 1178–1181, https://doi.org/10.1038/nature08985, 2010.

Thomas, Z., Abbott, B. W., Troccaz, O., Baudry, J., and Pinay, G.: Proximate and ultimate controls on carbon and nutrient dynamics of small agricultural catchments, Biogeosciences, 13, 1863–1875, https://doi.org/10.5194/bg-13-1863-2016, 2016.

Tong, R., Parajka, J., Salentinig, A., Pfeil, I., Komma, J., Széles, B., Kubáò, M., Valent, P., Vreugdenhil, M., Wagner, W., and Blöschl, G.: The value of ASCAT soil moisture and MODIS snow cover data for calibrating a conceptual hydrologic model, Hydrol. Earth Syst. Sci., 25, 1389–1410, https://doi.org/10.5194/hess-25-1389-2021, 2021.

Viaud, V., Santillàn-Carvantes, P., Akkal-Corfini, N., Le Guillou, C., Prévost-Bouré, N. C., Ranjard, L., and Menasseri-Aubry, S.: Landscape-scale analysis of cropping system effects on soil quality in a context of crop-livestock farming, Agr. Ecosyst. Environ., 265, 166–177, https://doi.org/10.1016/j.agee.2018.06.018, 2018.

Wang, A. and Solomatine, D. P.: Practical Experience of Sensitivity Analysis: Comparing Six Methods, on Three Hydrological Models, with Three Performance Criteria, Water, 11, 1062, https://doi.org/10.3390/w11051062, 2019.

Wang, S., Zhang, Z., Sun, G., Strauss, P., Guo, J., Tang, Y., and Yao, A.: Multi-site calibration, validation, and sensitivity analysis of the MIKE SHE Model for a large watershed in northern China, Hydrol. Earth Syst. Sci., 16, 4621–4632, https://doi.org/10.5194/hess-16-4621-2012, 2012.

Werth, S. and Güntner, A.: Calibration analysis for water storage variability of the global hydrological model WGHM, Hydrol. Earth Syst. Sci., 14, 59–78, https://doi.org/10.5194/hess-14-59-2010, 2010.

Winter, C., Lutz, S. R., Musolff, A., Kumar, R., Weber, M., and Fleckenstein, J. H.: Disentangling the Impact of Catchment Heterogeneity on Nitrate Export Dynamics From Event to Long-Term Time Scales, Water Resour. Res., 57, e2020WR027992, https://doi.org/10.1029/2020WR027992, 2021.

Woodward, S. J. R., Stenger, R., and Bidwell, V. J.: Dynamic analysis of stream flow and water chemistry to infer subsurface water and nitrate fluxes in a lowland dairying catchment, J. Hydrol., 505, 299–311, https://doi.org/10.1016/j.jhydrol.2013.07.044, 2013.

Woodward, S. J. R., Wöhling, T., Rode, M., and Stenger, R.: Predicting nitrate discharge dynamics in mesoscale catchments using the lumped StreamGEM model and Bayesian parameter inference, J. Hydrology, 552, 684–703, https://doi.org/10.1016/j.jhydrol.2017.07.021, 2017.

WRB: World reference base for soil resources, World soil resources reports, 103, 1–128, https://www.fao.org/fileadmin/templates/nr/images/resources/pdf_documents/wrb2007_red.pdf (last access: 19 December 2024), 2006.

Yadav, M., Wagener, T., and Gupta, H.: Regionalization of constraints on expected watershed response behavior for improved predictions in ungauged basins, Adv. Water Resour., 30, 1756–1774, https://doi.org/10.1016/j.advwatres.2007.01.005, 2007.

Yang, H., Choi, H., and Lim, H.: Applicability Assessment of Estimation Methods for Baseflow Recession Constants in Small Forest Catchments, Water, 10, 1074, https://doi.org/10.3390/w10081074, 2018.

Yassin, F., Razavi, S., Wheater, H., Sapriza-Azuri, G., Davison, B., and Pietroniro, A.: Enhanced identification of a hydrologic model using streamflow and satellite water storage data: A multicriteria sensitivity analysis and optimization approach, Hydrol. Process., 31, 3320–3333, https://doi.org/10.1002/hyp.11267, 2017.

Yen, H., Bailey, R. T., Arabi, M., Ahmadi, M., White, M. J., and Arnold, J. G.: The Role of Interior Watershed Processes in Improving Parameter Estimation and Performance of Watershed Models, J. Environ. Qual., 43, 1601–1613, https://doi.org/10.2134/jeq2013.03.0110, 2014.

Yeste, P., Melsen, L. A., García-Valdecasas Ojeda, M., Gámiz-Fortis, S. R., Castro-Díez, Y., and Esteban-Parra, M. J.: A Pareto-Based Sensitivity Analysis and Multiobjective Calibration Approach for Integrating Streamflow and Evaporation Data, Water Resour. Res., 59, e2022WR033235, https://doi.org/10.1029/2022WR033235, 2023.